GEOLOGICA CARPATHICA, APRIL 2020, 71, 2, 183–205 https://doi.org/10.31577/GeolCarp.71.2.6

U–Pb zircon geochronology and geochemistry of the metamorphic sole rocks of the Meydan mélange, South-East Turkey: Implications for ophiolite emplacement and protolith

NUSRET NURLU ✉

Çukurova University, Department of Geological Engineering, Balcalı, 01330 Adana, Turkey; ✉nusretnurlu@gmail.com

(Manuscript received November 15, 2019; accepted in revised form February 18, 2020; Associated Editor: Marian Janák)

Abstract: Metamorphic sole rocks at the base of the mantle tectonites of the Meydan ophiolite in South-East Anatolia, Turkey, are directly overlain by sheared serpentinites and cut by unmetamorphosed mafic dikes. They are found in areas close to the forefront of the Tauride thrust and are described as biotite amphibole schist (Bt+Hbl+Act+Plg+Rt±Zrn), prehnite–pumpellyite–amphibole schist (Prh+Pmp+Act+Plg±Rt±Ttn), amphibole schist (Fe^{2+}–Act+Qtz+Plg±Anl±Zrn), and amphibolite (Mg–Hbl+Plg±Zrn±Rt). They are identified as island arc tholeiites (IATs) based on their major- and trace-element whole-rock chemistry and mineral composition. The mafic dikes intruding into the metamorphic sole rocks and mantle tectonites exhibit tholeiitic affinity (Nb/Y=0.03–0.13) and are geochemically similar to island-arc basalts. The multiple elements, rare earth element (REE) trends, and related diagrams suggest that the mafic dikes were generated in a supra-subduction zone (SSZ) setting. Geothermobarometric examination based on the chemical compositions of the magnesio-hornblende in the amphibolites indicated that the pressure and temperature during the metamorphism were ~2.4 kbar (at depths of roughly 9 km) and ~630 °C, respectively. To elucidate the relationship and timing between the formation of the Meydan ophiolite and that of the metamorphic sole rocks, this paper presents new zircon U–Pb geochronological data from two samples of sole rocks, the ages of which are indicated to lie in the range of 81.4±0.69 Ma to 85.4±0.93 Ma (Santonian–Campanian). The precise U–Pb geochronology and the detailed petrographical and geochemical features of the metamorphic sole rocks and the protolith are evaluated to identify the tectonic environments of supra-subduction realms characterizing the South-Eastern Anatolian Orogenic Belt (SAOB). The metamorphic sole rocks were formed as a result of intra-oceanic thrusting during supra-subduction events in the basin throughout the closure of the SAOB in the Late Cretaceous.

Keywords: Metamorphic sole, Meydan mélange, South-East Anatolia, U–Pb geochronology, zircon.

Introduction

Metamorphic sole rocks consist of relatively high-grade metamorphic rocks, in association with ophiolites, and occur specifically at the local scale (e.g., Searle & Malpas 1980; Searle & Cox 2002). It is generally accepted that these metamorphic sole rocks were formed either as a result of low-angle shearing caused by over-thrusting of the oceanic plate in an oceanic setting (Williams & Smyth 1973; Jamieson 1980; Fergusson & Cawood 1994; Gartzos et al. 2009) or through a period of inceptive, intra-oceanic thrusting (Boudier et al. 1985). The obduction of oceanic crust through plate convergence is one of the most complicated geodynamic processes. Obducted fragments of the oceanic crust yield outcrops of ophiolites that enable the identification of the upper-mantle composition and evaluation of the duration and pressures of the processes by which the ophiolitic rocks were subducted at depth (Williams & Smyth 1973). Worldwide, metamorphic soles comprise thin sections of granulite and amphibolite facies, approximately 10–450 m in thickness, with variable proportions of sedimentary and basaltic material underlying most major ophiolites (Williams & Smyth 1973). Many researchers have reported the presence of metamorphic sole rocks beneath several ophiolitic complexes of the Tethys, including the Baer–Bassit in Syria (Al-Riyami et al. 2002), Mersin in Southern Turkey (Çelik 2008), and Pozanti–Karsantı in Turkey (Lytwyn & Casey 1995; Fig. 1a). The Semail in Oman is one of the best-preserved units of this type (Gnos & Peters 1993; Searle & Cox 2002). In addition, the Meydan mélange contains amphibolites of the metamorphic sole rocks in the South-Eastern Anatolian Orogenic Belt (SAOB). The Alpine–Himalayan orogeny was formed by the closure of the Neo-Tethyan Ocean, the convergence of Gondwana and Laurasia, and border defects throughout the Late Cretaceous. Anatolia is a significant segment of the Alpine–Himalayan orogenic system because it comprises considerable continental components and belts that emerged as a result of the collision of distinct branches of the Neo-Tethys Ocean from the Late Cretaceous to the Miocene (Şengör & Yılmaz 1981; Görür et al. 1984; Robertson & Dixon 1984; Poisson 1986; Okay & Tüysüz 1999). The Neo-Tethyan ophiolites located in Anatolia formed in east–west-oriented zones. These ophiolitic massifs are separated by sedimentary basins, metamorphic core complexes, and continental blocks around the northern margin of the Arabian foreland (Fig. 1b;

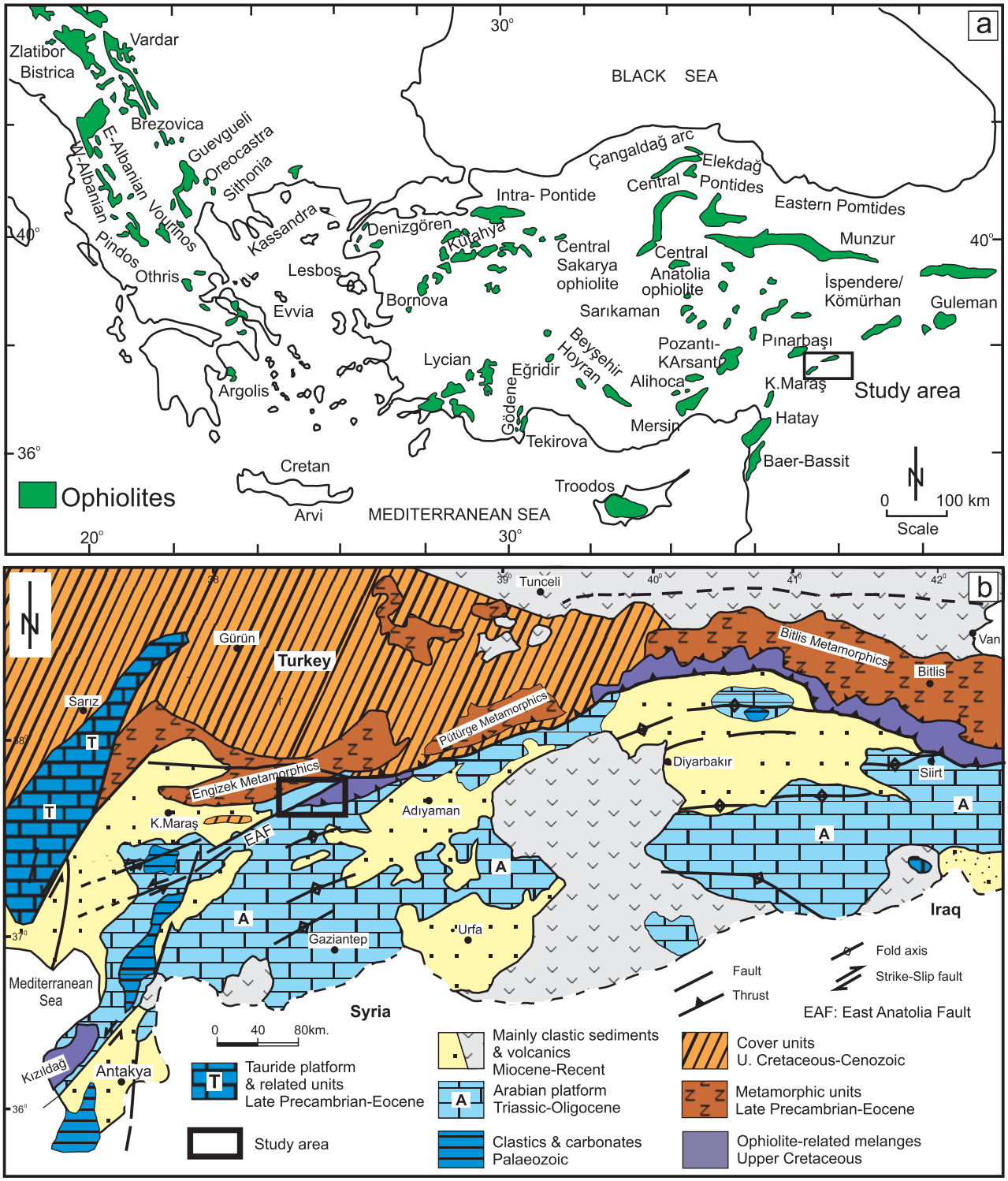

Fig. 1. A — Neo-Tethyan ophiolites in the Eastern Mediterranean region (from Robertson 2002; Rızaoğlu et al. 2006). **B** — Outline map of the Neotethyan ophiolites in the Eastern Mediterranean region, showing the study area (from Yılmaz 1993).

Şengör & Yılmaz 1981; Yılmaz 1993; Robertson et al. 2007). They show relicts of the Neo-Tethyan oceanic basins that were affected by a series of collisions of intra-oceanic, arc-trench systems with continental margins in the Cretaceous (Dilek et al. 1999; Dilek & Thy 2006).

The Late Cretaceous ophiolites of South-East Anatolia originated from the convergence of oceanic basins between the Eurasian and Afro–Arabian plates from the Late Triassic to the Late Cretaceous, which is characteristic for Neo-Tethyan sutures. From north to south, these suture zones are known as

(i) the İzmir–Ankara–Erzincan Suture Zone, (ii) the Inner Tauride Suture Zone, and (iii) the Bitlis–Zagros Suture Zone (Fig. 1a; Şengör & Yılmaz 1981; Robertson & Dixon 1984; Dilek & Moores 1990; Yılmaz 1993; Parlak & Robertson 2004; Robertson et al. 2007). Most researchers used petrographic and geochemical data to determine that the Neo-Tethyan ophiolitic extrusives and intrusives formed in a supra-subduction zone (SSZ) setting, (Pearce et al. 1984; Yılmaz 1993; Yalınız et al. 1996, 2000; Parlak & Delaloye 1999; Beyarslan & Bingöl 2000; Parlak et al. 2000, 2005, 2016; Robertson 2002, 2004; Çelik & Delaloye 2003). Metamorphic soles are believed to have formed during the first few million years of intra-oceanic subduction (Dewey 1976; Spray et al. 1984; Boudier et al. 1988; Hacker 1990; Dewey & Casey 2013), during which time, the ophiolitic crust of the subducted lithosphere was warmed by the accreted overlying mantle and pulled away from the upper plate, or the distant ophiolite. Coleman (1981) determined that the metamorphic sole rocks of the Semail ophiolite in Oman developed throughout the initiation of the obduction. The Eastern Mediterranean region includes metamorphic sole rocks related to ophiolites, namely the Meydan mélange. These rocks have been used to explain the pressure–temperature (P–T) conditions and the nature of the material accreted under the mantle tectonites, which were formed by intra-oceanic thrusting/subduction of the oceanic lithosphere (Önen & Hall 1993; Lanphere et al. 1975; Spray & Roddick 1980; Gnos & Peters 1993; Hacker 1994; Parlak 1996; Dilek et al. 1999). Several researchers have suggested the presence of metamorphic sole rocks beneath the Neo-Tethyan ophiolites in locations such as Pınarbaşı, Mersin, Divriği, and Kömürhan in Turkey as well as Semail in Oman (Fig. 1a; Searle & Cox 2002; Çelik & Delaloye 2003; Çelik et al. 2005; Parlak et al. 2005; Vergili & Parlak 2005; Kakar & Mahmood 2015; Roberts et al. 2016). The origin of these metamorphic sole rocks is constrained by the magma range proposed for the geodynamical environments of IAT, mid-ocean ridge basalt (MORB), and within-plate basalt (WPB; Önen & Hall 1993; Parlak 1996; Floyd et al. 2000; Çelik et al. 2004). The geochronology, petrography, field relationships, and geochemistry of the granitic and ophiolitic rocks occurring to the west of the Meydan region have been well defined in previous research (Parlak et al. 2004; Robertson et al. 2006, 2007; Nurlu 2009; Karaoğlan 2012). Nevertheless, reliable and systematic age data are still lacking for the protolith of the metamorphic sole rocks of the South-Eastern Anatolian ophiolite. Thus, the present study discusses the problem of metamorphic soles based on the present understanding of the genesis of ophiolite complexes and their role as tracers of supra-subduction realms. The main goal of this study was to identify the protolith, rates, and timing of recently investigated amphibolites constituting the metamorphic sole rocks and mafic dikes in the SAOB, South-East Turkey. The principal objectives of this research were to (i) determine the whole-rock major and trace element chemistries of the metamorphic sole rocks and mafic dike rocks; (ii) define the geodynamic setting, protolith, and geothermobarometric development of the metamorphic sole rocks, as well as the mineral data for these rocks; (ii) yield new U–Pb ages for amphibolites from these sole rocks; and (iv) summarize the geodynamic environment of the Meydan ophiolite during the development of the SAOB of the Neo-Tethyan oceanic region within the Eastern Mediterranean tectonic roof.

Geological background

One of the most spectacular orogenic belts was formed by the closure of the Neo-Tethys Ocean and runs from the Alps through the Middle East to the Himalayas (Fig. 1a). The study region holds an important but underexplored record of subduction and continental collision as the central part of an orogenic belt that stretches from the Alps to the Himalayas. The SAOB formed through the collision of the Afro–Arabian and Eurasian plates, following the closure of the southern Neo-Tethyan oceanic basin from the Cretaceous to the Miocene (Fig. 1b; Şengör & Yılmaz 1981). This orogenic belt contains numerous tectonomagmatic and stratigraphic units in the Kahramanmaraş–Adıyaman region, South-East Turkey, that are critical for understanding the tectonic and mineral resource evolution of Anatolia (Figs. 1b, 2a; Nurlu et al. 2016). The SAOB contains three different tectonic fragments trending roughly from east to west that have been separated by enormous north-dipping thrust faults (Figs. 1a,b, 2). From south to north, these units are defined as the Arabian platform carbonates, the zone of accretion, and the nappe zone (Yiğitbaş et al. 1992; Yılmaz 1993; Yılmaz et al. 1993). The nappe zone comprises two major sub-zones known as lower and upper nappes (Fig. 1b; Yılmaz 1993), which have been separated by a thrust zone from the south (Yigitbaş & Yılmaz 1996). The upper nappe is characterized by the Malatya, Bitlis, and Keban metamorphic massifs of South-East Anatolia, whereas the lower nappe primarily comprises variably metamorphosed and unmetamorphosed ophiolitic units, in addition to the Maden Group (Fig. 1b; Perinçek 1979; Ketin 1983; Yılmaz 1993; Elmas & Yılmaz 2003). The Arabian platform, which developed in a marine setting during the early Paleozoic to Miocene, presents a mostly autochthonous sedimentary succession (Yılmaz 1984; Perinçek & Fren 1990). In South-East Anatolia, distinct ophiolitic bodies obducted onto the Arabian platform during the Late Cretaceous to the Eocene (Fig. 1; Perinçek 1979; Yigitbaş et al. 1992). Although this region is largely underexplored, it forms a crucial record of continental collision and subduction in the central part of an orogenic belt that stretches from the Himalayas to the Alps. The SAOB contains crucial examples of unmetamorphosed ophiolites; listed from west to east; these include the Göksun, Meydan (Kahramanmaraş), İspendere, Kömürhan (Malatya), and Guleman (Elazığ) ophiolites in the northern region and the Koçali (Adıyaman) and Kızıldağ (Hatay) ophiolites in the south (Fig. 1; Yazgan & Chessex 1991; Yılmaz 1993; Yılmaz et al. 1993; Beyarslan & Bingöl 2000; Parlak et al. 2004; Bağcı et al. 2005, 2008; Rızaoğlu et al. 2006; Robertson et al.

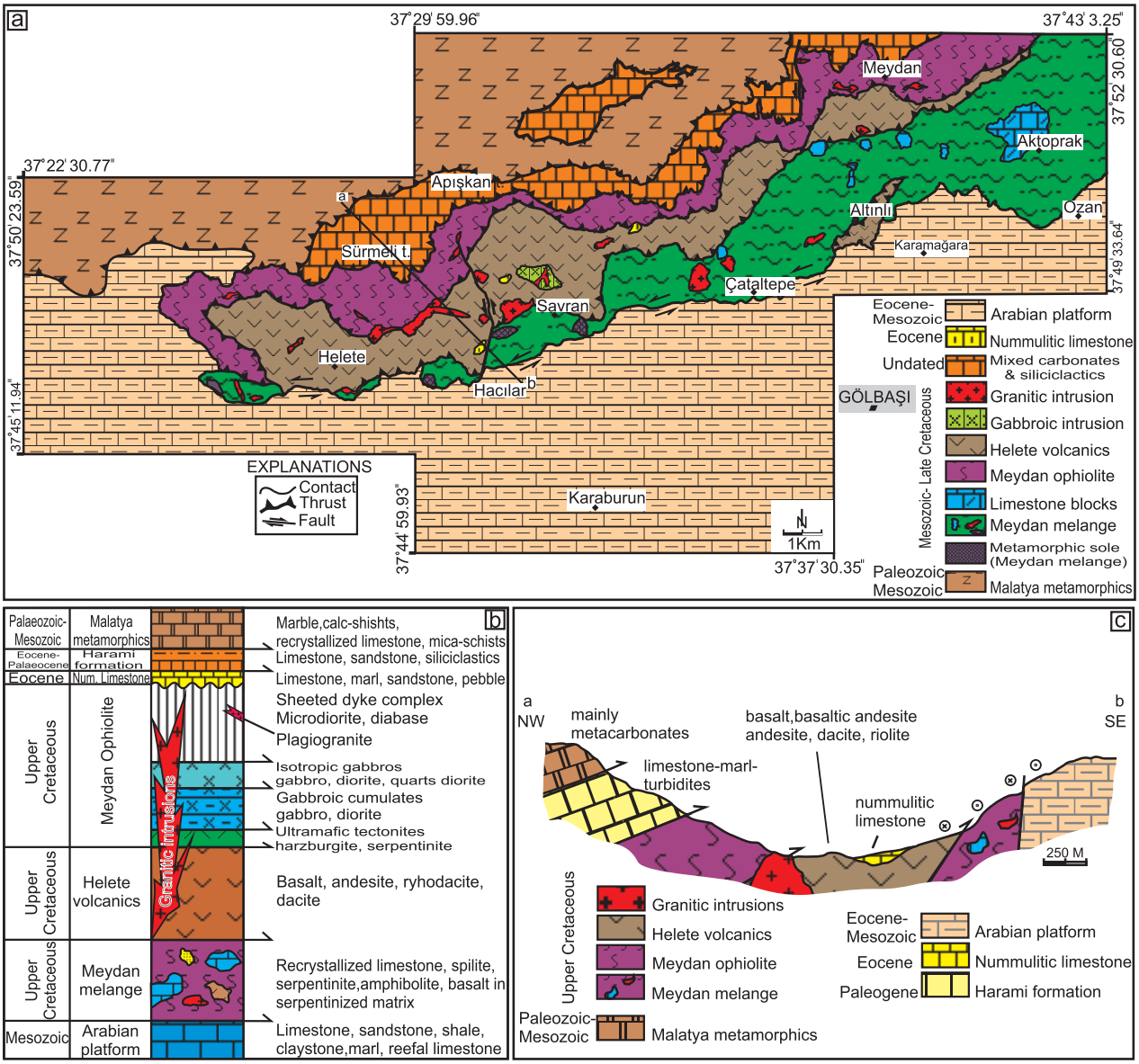

Fig. 2. A — Geological map of the study area based on this work (Nurlu 2016). **B** — Tectonostratigraphy of studied area. **C** — Cross section summarizing the field relations of the units.

2006, 2007; Parlak et al. 2009; Nurlu 2016; Nurlu et al. 2016; Özek et al. 2017). These ophiolitic bodies present a complete ophiolite pseudo-stratigraphy and are overlain by the Late Cretaceous to early Cenozoic Harami Formation, as well as a slice of mixed complex carbonate–clastic rocks composed of marl, limestone, and gravity-flow deposits. A zone of imbrication is observed throughout the Arabian platform carbonates and includes a nappe stack composed of Late Cretaceous to Miocene volcanic and sedimentary units (Fig. 2b,c; Yılmaz et al. 1993; Elmas & Yılmaz 2003). The Helete–Gölbaşı area contains numerous tectonomagmatic/metamorphic and stratigraphic units, which are crucial for determining the development of the southern branch of the Neo-Tethyan Ocean from the Late Cretaceous to early Cenozoic times. These units include i) the Malatya–Keban metamorphic units, which make up the Harami Formation and form part of a carbonate–clastic rock complex composed of marl, limestone, recrystallized limestone, and gravity-flow deposits; ii) unmetamorphosed ophiolitic rocks, which are known regionally as the Meydan ophiolite; iii) Helete volcanics (Helete Group); iv) an ophiolite-associated mélange, which is known locally as the Meydan mélange; v) granitic intrusions; and vi) Arabian platform carbonates. The granitic rocks in the Adıyaman–Kahramanmaraş region are composed mostly of granitic, tonalitic, and granodioritic rocks. The granites and tonalites include numerous gabbroic–dioritic mafic microgranular enclaves of several sizes. The granites, granodiorites, and tonalites have distinct geochemical characteristics of calc–alkaline volcanic arc rocks (Fig. 2a,c; Parlak 2006; Nurlu et al. 2016). The metamorphic sole rocks of the Meydan ophiolite are intruded by

synkinematic mafic dikes near Savran village. The ubiquitous presence of chilled margins indicates that these mafic dikes contain synkinematic minerals rather than blocks. The Meydan mélange is related to the ophiolite and comprises amphibolite, serpentinized ultramafic rock, gabbro, spilitic basalt, and recrystallized limestone. The metamorphic sole rocks observed in the Meydan mélange were accreted beneath the base of the Meydan ophiolite, the subduction characteristics of which were presented by Nurlu (2016). The IAT characteristics of the metamorphic sole rocks at the base of the SAOB ophiolite are most likely associated with basalts of an SSZ-type ophiolite (Rızaoğlu et al. 2006; Nurlu 2016). The amphibolites of the metamorphic sole rocks form an outcrop in the south-eastern region, particularly to the south of Helete and Savran villages (Fig. 2a). The Late Cretaceous ages for the Meydan ophiolite, the intruded granitic rocks in the Helete volcanics, the Meydan ophiolite, and the boundary between them suggest that the existing interpretation of an Eocene age for the Helete volcanic unit can be ruled out and that the Meydan ophiolite age extends from the Late Cretaceous to the Eocene (Nurlu 2016; Nurlu et al. 2016). On the basis of this evidence, it is believed that the Helete volcanics represent volcanic rocks of the Meydan ophiolite. The mélange contains sheets of serpentinized ultramafic rocks and severely sheared blocks of amphibolite, spilitic basalt, mafic dikes, gabbro, and recrystallized limestone (Fig. 2a–c). The Meydan mélange exhibits a block-against-block structure and shows no evidence of a sedimentary matrix. Relatively competent gabbro, radiolarite, and massive marble form subangular to angular blocks up to tens of metres in size (Nurlu et al. 2016). Remarkable metamorphic sole units are seen in the Meydan mélange to the north (Çataltepe) and to the south of Savran village (Fig. 2a).

Analytical methods

Petrographical analyses

The metamorphic sole and mafic dike rock types were initially examined in thin section handling an optical microscope (ca. 85 thin sections) and rocks suitable for petrological analysis were sampled.

Major and trace element analyses

A total of 9 samples of metamorphic sole rocks and 2 samples of mafic dikes were analysed for major and trace elements. Whole-rock geochemistry of samples M-74, M-22, M-184, M-185, M-6, M-8, M-4(MG-1), M-5(MG-2) (metamorphic sole is dated), M-2 (metamorphic sole rocks), MD-1, MD-2 (mafic dikes) were determined at the ACME Analytical Laboratories Ltd. in Vancouver (Canada). Total abundances of the major oxides were obtained by ICP-OES (Inductively Coupled Plasma Optical Emission Spectroscopy), and trace elements by ICP-MS (Mass Spectroscopy). Sample preparations follow a $LiBO_2$ fusion and dilute nitric digestion for major oxides, rare earth elements and refractory elements, whereas precious and base metals were digested in acquaregia. Prepared sample is mixed with $LiBO_2/Li_2B_4O_7$ flux. Crucibles are fused in a furnace. The cooled bead is dissolved in ACS grade nitric acid and analysed by ICP-OES and/or ICP-MS. Loss on ignition (LOI) is determined by igniting a sample split then measuring the weight loss. Total Carbon and Sulphur may be included and is determined by the Leco method (TC003). The LF202 package includes an additional 14 elements from an aqua regia digestion AQ200 to provide Au and volatile elements which do not report as part of the LF200 package. Representative data are shown in Table 1.

Electron microprobe analyses

Thin sections (about 30 microns thick) for four samples were prepared by the EAS Thin Section Laboratory at the Department of Earth and Atmospheric Sciences (EAS) at the University of Alberta. Major element compositions of minerals and phase relationships were studied by electron microprobe at the EAS at the University of Alberta (Canada). The operating conditions were; 40 degrees take off angle, accelerating voltage 20 kV, beam current 20 nA, and beam diameter <1 micron (fully focused), except on the zeolite points that were run separately with a 10 micron diameter beam. The Kα X-ray lines of 13 elements were measured using the following diffraction crystals: PET (pentaerythritol) – P, K, Ca, Ti, V, Cr; TAP (thallium hydrogen phthalate) – Na, Mg, Al, Si; LIF (lithium fluoride) – Mn, Fe, Ni. Total count times of 30 seconds were used for both emission peaks and background positions for all elements except Na, for which 60 seconds was used. Interference corrections were applied to V for interference by Ti, and to Cr for interference by V, and to Mn for interference by Cr (Donovan et al. 1993). Intensity data were reduced according to Armstrong (1988) and the choice of mineral standards varied with the mineral analysed. Oxygen was calculated by stoichiometry and included in the data reduction. Representative data are shown in Tables 2–4.

LA-ICP-MS Zircon U–Pb Analyses

Sample preparation and imaging

Zircons were isolated from the amphibolites (MG1–MG2) by mineral separation techniques at Çukurova University Geological Department, making use of standard methods (i.e., crushing, milling, magnetic separation, heavy liquid separation and hand-picking under a binocular microscope).

Zircon samples were embedded in 25 mm epoxy resin discs and polished to expose the interior of the mineral grains. All zircons were CL-imaged prior to LA U–Pb work using a Zeiss Merlin scanning electron microscope (SEM) equipped with a CL detector at the Central Analytical Facilities, Stellenbosch University (South Africa). A detailed explanation of LA-ICP-MS methods is given in Supplementary Table S1.

Petrography and mineralogy

The Meydan ophiolite contains a complete ophiolitic sequence that includes mantle tectonites, ultramafic and mafic cumulates, isotropic gabbros, rare sheeted dikes, and volcaniclastics (Figs. 2, 3; Nurlu 2016; Nurlu et al. 2016). The tectonites are dominated by serpentinized harzburgite and minor pyroxenite. The intrusions of mafic dikes in the harzburgitic

Table 1: Major and trace element analyses of the amphibolites and mafic dikes.

Sample	M-74	M-22	M-184	M-185	M-6	M-8	M-4	M-5	M-2	M-D-1	M-D2
Rokc Type	Metamorphic rocks									Mafic dikes	
SiO_2	49.4	49.8	49.7	51.6	46.4	51.2	46.8	48.7	52.5	42.2	42.8
Al_2O_3	16.6	12.2	17.3	17.0	12.5	15.1	10.8	13.2	15.2	16.9	16.8
Fe_2O_3*	10.1	8.6	9.8	9.2	6.0	4.4	5.8	5.4	6.9	8.5	8.4
MgO	6.93	10.70	6.58	6.10	6.57	7.14	7.31	10.90	5.64	8.24	8.67
CaO	10.5	10.4	10.3	10.0	17.4	10.7	18.3	10.6	11.2	16.9	16.6
Na_2O	2.77	1.86	2.77	2.97	1.99	4.44	2.48	3.01	2.89	0.51	0.47
K_2O	0.69	2.24	1.01	0.76	0.41	0.57	0.36	0.44	0.99	0.19	0.21
TiO_2	0.76	0.52	0.78	0.73	0.53	0.66	0.43	0.46	0.55	0.74	0.69
P_2O_5	0.08	0.08	0.08	0.06	0.04	0.05	0.04	0.04	0.05	0.09	0.08
MnO	0.18	0.15	0.17	0.17	0.11	0.08	0.11	0.10	0.13	0.13	0.14
Cr_2O_3	0.019	0.076	0.014	0.012	0.030	0.029	0.043	0.067	0.010	0.011	0.013
Ni	35	165	46	27	70	125	98	283	30	78	83
Sc	40	39	37	35	26	29	24	23	30	25	32
LOI	1.8	3.1	1.4	1.3	7.7	5.3	7.3	6.8	3.7	5.4	5.2
Sum	99.87	99.8	99.84	99.87	99.8	99.79	99.81	99.74	99.84	99.8	99.8
Ba	106	562	174	124	455	220	506	202	201	34	48
Be	3	3	1	<	<	<	<	<	<	<	<
Co	32.7	40.7	32.9	28.5	25.4	24.0	25.7	32.2	26.9	27.5	29.2
Cs	0.2	1.0	<	<	0.3	<	0.1	0.4	0.2	0.2	0.2
Ga	14.5	9.7	13.6	14.1	7.8	10.2	9.2	9.3	13.3	12.6	11.8
Hf	1.2	1.1	1.4	0.9	1.1	1.4	0.9	1.4	1.4	1.5	1.4
Nb	0.6	0.5	0.7	0.6	1.0	1.7	0.8	2.4	1.8	1.3	1.2
Nb/Y	0.03	0.04	0.04	0.04	0.07	0.11	0.07	0.13	0.11	0.08	0.08
Rb	8.4	23.5	15.3	8.8	6.6	8.7	7.7	7.2	10.1	3.3	3.8
Sn	<	<	<	<	2	<	<	1	<	<	<
Sr	164.2	373.2	176.7	149.6	372.0	373.2	287.9	343.2	184.3	42.5	57.2
Ta	<	<	<	<	<	<	<	0.20	0.10	<	<
Th	<	0.7	<	0.2	0.6	1.3	0.5	1.2	1.1	0.5	0.4
U	<	0.2	0.1	0.2	0.5	0.7	0.3	0.4	0.8	0.2	0.2
V	311	209	294	284	179	211	163	161	195	213	198
W	25.10	6.90	4.60	6.20	<	<	<	0.80	<	<	<
Zr	36.7	29.3	39.9	36.2	40.8	44.5	34.1	42.0	43.1	57.8	61.8
Y	19.0	12.9	16.2	16.9	14.5	15.2	11.9	18.3	16.5	16.5	15.8
La	2.9	5.8	2.5	2.9	3.8	5.3	3.1	5.1	4.5	5.6	5.8
Ce	7.5	11.6	6.6	6.8	8.3	10.4	5.9	11.7	9.4	12.6	12.4
Pr	1.06	1.50	1.03	0.98	1.04	1.21	0.78	1.46	1.18	1.67	1.51
Nd	5.80	6.30	5.10	4.60	5.10	5.50	3.90	6.60	5.20	8.20	7.90
Sm	1.46	3.50	1.44	1.09	1.44	1.32	1.26	1.92	1.60	2.10	2.14
Eu	0.73	0.64	0.67	0.66	0.51	0.42	0.44	0.49	0.55	0.82	0.79
Gd	2.62	1.96	2.26	2.25	1.77	2.06	1.59	2.28	2.13	2.74	2.77
Tb	0.44	0.32	0.42	0.41	0.35	0.36	0.29	0.45	0.40	0.47	0.44
Dy	2.89	2.14	2.79	2.72	2.41	2.56	2.01	3.17	2.64	2.91	2.95
Ho	0.65	0.43	0.60	0.61	0.52	0.56	0.49	0.68	0.65	0.67	0.65
Er	2.10	1.31	1.75	1.83	1.76	1.71	1.41	2.12	1.85	2.07	2.13
Tm	0.25	0.18	0.26	0.22	0.23	0.26	0.21	0.32	0.28	0.28	0.29
Yb	2.03	2.21	1.91	1.72	1.67	1.83	1.51	2.41	2.03	1.98	1.93
Lu	0.30	0.21	0.25	0.24	0.24	0.27	0.21	0.39	0.30	0.29	0.27
TOT/C	0.06	0.08	0.03	0.04	0.28	0.20	0.35	0.26	0.32	0.03	0.03
TOT/S	<	<	<	<	<	<	<	<	0.02	<	<
Mo	1.2	0.3	1.8	<	<	0.1	<	0.2	0.1	<	<
Cu	26.8	41.2	85.4	65.1	57.3	11.1	26.1	56.0	35.5	46.4	44.2
Pb	0.9	0.7	0.6	0.4	0.6	0.4	1.2	0.5	0.9	0.4	0.7
Zn	15	8	14	17	3	3	5	3	10	10	12
Ni	17.2	32.4	28.9	15.7	20.8	24.3	30.7	65.7	12.0	66.0	66.2
Mg#	34.8	49.0	34.3	34.1	45.9	55.7	49.4	60.9	38.8	42.8	44.4
La_N/Yb_N	1.02	1.84	0.50	1.29	1.35	1.27	0.71	1.03	1.05	1.28	1.06

< Below detection limit; Fe is expressed as FeO* (Mg#=100*Mg/(Mg+Fe^+total))

Table 2: Composition of the amphibole from the metamorphic sole rocks.

Rock Type	Amphibolite														
Type	Group I														
SAMPLE	M4-1	M4-2	M4-3	M4-4	M4-5	M4-6	M4-7	M4-8	M4-9	M4-10	M4-11	M4-12	M4-13	M4-14	M4-15
SiO_2	49.32	50.02	50.27	50.54	49.41	48.04	48.81	45.09	45.61	49.79	49.58	49.27	44.35	49.56	48.87
TiO_2	0.65	0.65	0.69	0.55	0.72	0.87	0.67	0.58	0.67	0.61	0.56	0.64	0.59	0.61	0.59
Al_2O_3	6.92	6.03	6.06	5.94	6.85	7.44	6.87	10.97	10.42	6.60	6.93	7.19	11.18	6.46	7.40
Cr_2O_3	0.03	0.00	0.00	0.00	0.07	0.00	0.08	0.06	0.24	0.09	0.05	0.06	0.05	0.13	0.17
MnO	0.25	0.27	0.24	0.23	0.21	0.27	0.26	0.26	0.25	0.26	0.24	0.26	0.27	0.26	0.25
FeO	11.02	11.00	10.74	10.35	10.99	11.72	11.31	12.61	12.18	10.34	10.37	10.76	12.95	10.98	10.86
MgO	15.15	15.43	15.66	15.78	15.10	14.30	14.88	12.67	13.06	15.48	15.09	14.94	12.94	15.15	14.82
CaO	12.48	12.45	12.48	12.48	12.45	12.39	12.43	12.29	12.30	12.56	12.51	12.47	11.80	12.41	12.45
Na_2O	0.78	0.76	0.66	0.66	0.85	0.84	0.72	1.24	1.17	0.72	0.69	0.78	1.25	0.77	0.84
K_2O	0.35	0.30	0.32	0.25	0.38	0.41	0.42	0.41	0.44	0.31	0.29	0.37	0.52	0.34	0.34
Initial Total	96.95	96.93	97.12	96.81	97.03	96.31	96.51	96.22	96.37	96.78	96.31	96.77	95.92	96.71	96.63
Normalization Scheme: 13-CNK, all ferrous iron															
Si	7.140	7.238	7.243	7.290	7.157	7.044	7.114	6.660	6.716	7.201	7.208	7.149	6.555	7.196	7.107
Al	0.860	0.762	0.757	0.710	0.843	0.956	0.886	1.340	1.284	0.799	0.792	0.851	1.445	0.804	0.893
ΣT	8.000	8.000	8.000	8.000	8.000	8.000	8.000	8.000	8.000	8.000	8.000	8.000	8.000	8.000	8.000
Ti	0.071	0.071	0.075	0.060	0.078	0.096	0.073	0.064	0.074	0.066	0.061	0.070	0.066	0.067	0.065
Al	0.321	0.267	0.272	0.300	0.327	0.329	0.294	0.569	0.524	0.326	0.395	0.379	0.502	0.301	0.375
Cr	0.003	0.000	0.000	0.000	0.008	0.000	0.009	0.007	0.028	0.010	0.006	0.007	0.006	0.015	0.020
Fe^{3+}	0.179	0.160	0.170	0.136	0.114	0.177	0.217	0.261	0.231	0.128	0.079	0.103	0.490	0.149	0.134
Zn							0.003								
Mn^{2+}	0.001	0.001	0.000	0.000	0.000	0.009	0.005	0.007	0.004	0.007	0.007	0.003	0.000	0.000	0.003
Fe^{2+}	1.156	1.171	1.119	1.108	1.212	1.260	1.162	1.296	1.269	1.122	1.182	1.203	1.083	1.184	1.187
Mg	3.270	3.329	3.364	3.393	3.261	3.126	3.233	2.790	2.867	3.338	3.270	3.232	2.851	3.279	3.213
ΣC	5.001	5.001	5.000	5.000	5.000	5.001	5.000	4.999	5.001	4.999	5.000	5.001	5.000	5.000	5.002
Mn^{2+}	0.030	0.032	0.029	0.028	0.026	0.025	0.027	0.026	0.028	0.025	0.022	0.029	0.034	0.032	0.028
Ca	1.936	1.930	1.927	1.929	1.932	1.946	1.941	1.945	1.941	1.946	1.949	1.939	1.869	1.931	1.940
Na	0.034	0.037	0.039	0.038	0.036	0.029	0.031	0.029	0.032	0.029	0.029	0.033	0.070	0.037	0.032
ΣB	2.000	1.999	2.000	2.000	2.000	2.000	1.999	2.000	2.001	2.000	2.000	2.001	2.001	2.000	2.000
Na	0.185	0.176	0.145	0.147	0.203	0.210	0.172	0.326	0.302	0.173	0.165	0.187	0.288	0.180	0.205
K	0.065	0.055	0.059	0.046	0.070	0.077	0.078	0.077	0.083	0.057	0.054	0.068	0.098	0.063	0.063
ΣA	0.250	0.231	0.204	0.193	0.273	0.287	0.250	0.403	0.385	0.230	0.219	0.255	0.386	0.243	0.268
O (non-W)	22.00	22.00	22.00	22.00	22.00	22.00	22.00	22.00	22.00	22.00	22.00	22.00	22.00	22.00	22.00
W (OH)	2.000	2.000	2.000	2.000	2.000	2.000	2.000	2.000	2.000	2.000	2.000	2.000	2.000	2.000	2.000
W subtotal	2.000	2.000	2.000	2.000	2.000	2.000	2.000	2.000	2.000	2.000	2.000	2.000	2.000	2.000	2.000
Σ (T,C,B,A)	15.251	15.231	15.204	15.193	15.273	15.288	15.249	15.402	15.387	15.229	15.219	15.257	15.387	15.243	15.270
Species	Mg-Hb	Mg-Hb	Mg-Hb	Mg-Hb	Mg-Hb	Mg-Hb	Mg-Hb	Mg-Hb	Mg-Hb	Mg-Hb	Mg-Hb	Mg-Hb	Mg-Hb	Mg-Hb	Mg-Hb
Al_{tot}	1.181	1.029	1.029	1.010	1.170	1.285	1.180	1.909	1.808	1.125	1.187	1.230	1.947	1.105	1.268
P kbar (b) [±0.5 kb]	2.2786982	1.8941458	1.8941458	1.8493095	2.2493255	2.5683039	2.276018	4.7579386	4.3509677	2.1316719	2.2948212	2.4124655	4.916312	2.0806749	2.5194929
T (°C) (c) [±30 °C]	629.9	629.9	634.7	616.6	639.1	660.1	633.2	622.3	634.2	624.7	618.5	628.8	623.7	625.0	622.5

Number of ions on the basis of 23 oxygens. Total Fe is expressed as FeO*.

Table 2 (continued): Composition of the amphibole from the metamorphic sole rocks.

Rock Type	Amphibolite															
Type	Group I											Group II				
SAMPLE	M4-15	M4-16	M4-17	M4-18	M4-19	M4-20	M4-26	M4-27	M4-28	M4-29	M4-30	M4-21	M4-22	M4-23	M4-24	M4-25
SiO_2	48.87	45.48	49.47	44.83	49.49	45.81	44.09	45.59	50.10	45.84	49.62	52.51	52.56	53.92	53.28	53.55
TiO_2	0.59	0.56	0.57	0.64	0.64	0.52	0.73	0.65	0.71	0.66	0.71	0.00	0.00	0.03	0.02	0.02
Al_2O_3	7.40	10.38	6.66	10.88	6.33	10.12	11.58	10.38	6.16	9.93	6.17	0.36	0.25	0.46	0.33	0.54
Cr_2O_3	0.17	0.12	0.06	0.05	0.14	0.05	0.00	0.06	0.07	0.06	0.06	0.00	0.00	0.00	0.00	0.03
MnO	0.25	0.22	0.23	0.27	0.27	0.25	0.24	0.25	0.26	0.25	0.26	0.71	0.75	0.51	0.54	0.59
FeO	10.86	12.81	11.17	13.25	11.35	12.55	13.48	12.93	10.61	12.61	11.34	21.55	21.80	18.67	20.42	19.46
MgO	14.82	12.84	15.11	12.64	14.92	13.34	11.55	12.60	15.24	12.86	15.01	8.61	8.39	10.94	9.77	10.38
CaO	12.45	12.39	12.54	12.33	12.38	12.37	12.31	12.30	12.39	12.28	12.34	12.90	12.63	12.87	12.66	12.91
Na_2O	0.84	1.13	0.73	1.28	0.70	1.15	1.21	1.12	0.76	1.05	0.71	0.03	0.03	0.04	0.05	0.00
K_2O	0.34	0.50	0.27	0.44	0.34	0.49	0.56	0.45	0.31	0.42	0.30	0.05	0.03	0.04	0.02	0.01
Initial Total	96.63	96.47	96.85	96.64	96.59	96.68	95.80	96.36	96.63	95.99	96.55	96.72	96.44	97.48	97.09	97.49
Normalization Scheme: 13-CNK, all ferrous iron																
Si	7.107	6.706	7.168	6.609	7.204	6.721	6.593	6.733	7.267	6.782	7.221	7.998	8.032	8.006	8.015	7.987
Al	0.893	1.294	0.832	1.391	0.796	1.279	1.407	1.267	0.733	1.218	0.779	0.002	0.000	0.000	0.000	0.013
ΣT	8.000	8.000	8.000	8.000	8.000	8.000	8.000	8.000	8.000	8.000	8.000	8.000	8.032	8.006	8.015	8.000
Ti	0.065	0.062	0.062	0.071	0.070	0.057	0.082	0.072	0.077	0.073	0.078	0.000	0.000	0.003	0.002	0.002
Al	0.375	0.510	0.305	0.499	0.290	0.471	0.634	0.540	0.320	0.513	0.279	0.063	0.045	0.080	0.059	0.082
Cr	0.020	0.014	0.007	0.006	0.016	0.006	0.000	0.007	0.008	0.007	0.007	0.000	0.000	0.000	0.000	0.000
Fe^{3+}	0.134	0.274	0.197	0.352	0.163	0.329	0.181	0.228	0.081	0.228	0.163	0.000	0.000	0.000		0.000
Zn		0.004		0.003			0.003									
Mn^{2+}	0.003	0.008	0.003	0.009	0.001	0.005	0.018	0.006	0.009	0.006	0.000	0.092	0.097	0.064	0.069	0.075
Fe^{2+}	1.187	1.305	1.156	1.282	1.219	1.211	1.505	1.369	1.206	1.332	1.214	2.745	2.786	2.318	2.569	2.427
Mg	3.213	2.822	3.264	2.778	3.238	2.918	2.575	2.774	3.296	2.836	3.256	1.955	1.911	2.421	2.191	2.308
ΣC	5.002	4.999	4.999	5.000	5.001	5.001	5.000	5.000	4.999	4.999	5.001	4.855	4.839	4.886	4.890	4.898
Mn^{2+}	0.028	0.020	0.025	0.024	0.032	0.026	0.013	0.025	0.023	0.025	0.032	0.000	0.000	0.000	0.000	0.000
Ca	1.940	1.957	1.947	1.948	1.931	1.944	1.972	1.946	1.926	1.947	1.924	2.000	2.000	2.000	2.000	2.000
Na	0.032	0.023	0.028	0.028	0.037	0.030	0.015	0.029	0.051	0.029	0.041					
ΣB	2.000	2.000	2.000	2.000	2.000	2.000	2.000	2.000	2.000	2.001	2.000	2.000	2.000	2.000	2.000	2.000
Na	0.205	0.300	0.177	0.338	0.161	0.297	0.336	0.292	0.162	0.273	0.160	0.009	0.009	0.012	0.015	0.000
K	0.063	0.094	0.050	0.083	0.063	0.092	0.107	0.085	0.057	0.079	0.056	0.010	0.006	0.008	0.004	0.002
ΣA	0.268	0.394	0.227	0.421	0.224	0.389	0.443	0.377	0.219	0.352	0.216	0.124	0.083	0.067	0.059	0.065
O (non-W)	22.00	22.00	22.00	22.00	22.00	22.00	22.00	22.00	22.00	22.00	22.00	22.00	22.00	22.00	22.00	22.00
W (OH)	2.000	2.000	2.000	2.000	2.000	2.000	2.000	2.000	2.000	2.000	2.000	2.000	2.000	2.000	2.000	2.000
W subtotal	2.000	2.000	2.000	2.000	2.000	2.000	2.000	2.000	2.000	2.000	2.000	2.000	2.000	2.000	2.000	2.000
Σ (T,C,B,A)	15.270	15.393	15.226	15.421	15.225	15.390	15.443	15.377	15.218	15.352	15.217	14.979	14.954	14.959	14.964	14.963
Species	Mg-Hb	Mg-Hb	Mg-Hb	Mg-Hb	Mg-Hb	Mg-Hb	Mg-Hb	Mg-Hb	Mg-Hb	Mg-Hb	Mg-Hb	Fe-Act	Fe-Act	Act	Fe-Act	Fe-Act
Al_{tot}	1.268	1.804	1.137	1.890	1.086	1.750	2.041	1.807	1.053	1.731	1.058	0.065	0.045	0.080	0.059	0.095
P kbar (b) [±0.5 kb]	2.5194929	4.3352679	2.1626522	4.6798295	2.032965	4.1264375	5.3204236	4.3470398	1.951808	4.0543402	1.9639652	0.5257189	0.5169099	0.532848	0.5229926	0.540425
T (℃) (c) [±30℃]	622.5	619.6	619.6	630.2	629.2	613.9	643.5	631.7	638.0	633.1	638.3	545.0	545.0	549.0	547.7	547.7

Number of ions on the basis of 23 oxygens. Total Fe is expressed as FeO*.

tectonites of the Meydan ophiolite and its metamorphic sole are narrow and are represented as diabase and microgabbro (Fig. 4g,h).

Four rock types have been observed in the metamorphic sole of the Meydan mélange: (i) amphibolite, (ii) amphibole schist, (iii) biotite amphibole schist, and (iv) prehnite–pumpellyite–amphibole schist. The metamorphic sole rocks exhibit grano-nematoblastic, granoblastic, porphyroblastic, and porphyro-nematoblastic textures (Fig. 4a–d,f).

These amphibolites include solely green–brown hornblende and show no marked foliation (Fig. 4a). Some of the representative amphibolite samples have relict textures, such as ophitic texture (Fig. 4a), which were inherited from the microgabbro original rocks and survived retrograde metamorphism. These features include tabular plagioclase crystals, heterogeneous grains sizes, and scarcity of the 120° conjunction. The foliation observed in the metamorphic sole rocks is widespread and is dominated by the foliation of actinolite–plagioclase and amphibole–plagioclase–biotite–quartz. The actinolite schist exhibits a grano-nematoblastic texture and is composed of 55–70 % actinolite, 15–20 % plagioclase, 2–4 % chlorite, and opaque minerals such as pyrite and magnetite (Fig. 4b). The amphibole schist exhibits a nematoblastic texture and displays clear foliation as a result of the preferred orientation of the amphiboles (Fig. 4b,d). The biotite amphibole schist (MG-1/MG-2) is composed of 7–9 % biotite, 13–15 % plagioclase, 5–7 % actinolite, and 67–69 % hornblende and exhibits nematoblastic and porphyroblastic textures (Fig. 4c,f). This schist also includes accessory minerals such as zircon, rutile, titanite, and apatite (Fig. 4c), as well as small amounts of opaque minerals in the disseminated form. The prehnite–pumpellyite–amphibole schist contains 5–7 % prehnite, 3–4 % pumpellyite, 11–15 % plagioclase, and 65–72 % hornblende and exhibits nematoblastic and porphyroblastic textures (Fig. 4d). The actinolite schist presents a greenschist facies and a porphyro-nematoblastic texture. These rocks are composed of 2–7 % plagioclase, 7–9 % quartz, and 65–68 % actinolite and include accessory minerals such as apatite, rutile, and zircon; veins have been filled by analcime and tobermorite, each at 2–3 % (Fig. 4d).

The mafic dikes in the Meydan mélange exhibit fine-grained textures and generally consist of 27–35 % clinopyroxene, 5–12 % green to brown hornblende, 3–4 % biotite, 40–42 % plagioclase and secondary minerals such as rare quartz, chlorite, and albite (Fig. 4e). The thicknesses of these dikes range from 30 cm to 50 cm, and they display clear chilled margins and intergranular, subophitic textures. Reaction rims of green–brown amphiboles surround relict grains of clinopyroxene; most of these amphiboles were transformed from clinopyroxenes (Fig. 4e).

U–Pb geochronology

A crucial objective of this research is to define protolith ages for the metamorphic sole rocks of the Meydan mélange to elucidate their spatial and temporal relationships. High-precision

Table 3: Composition of the biotite mineral from metamorphic sole rocks.

Rock Type	Biotite amphibole schist									
SAMPLE	M4-B1	M4-B2	M4-B3	M4-B4	M4-B5	M4-B6	M4-B7	M4-B8	M4-B9	M4-B10
SiO_2	37.51	37.47	37.41	37.02	37.21	36.92	37.18	37.33	37.07	36.98
TiO_2	2.51	2.51	2.43	2.48	2.49	2.88	2.84	2.79	2.79	2.68
Al_2O_3	16.62	16.67	16.43	16.45	16.3	15.79	15.93	16	16	16.01
Cr_2O_3	0.28	0.34	0.33	0.38	0.37	0.33	0.33	0.36	0.32	0.29
FeO	13.06	13.16	13.04	13.02	13.09	13.84	13.97	13.76	13.76	13.77
MnO	0.12	0.12	0.12	0.13	0.11	0.13	0.13	0.14	0.13	0.11
MgO	15	15.05	14.97	14.79	14.78	14.57	14.51	14.67	14.66	14.68
CaO	0.04	0.06	0.03	0.05	0.05	0.05	0.02	0	0.01	0.03
Na_2O	0.25	0.22	0.32	0.29	0.26	0.24	0.23	0.24	0.24	0.24
K_2O	9.69	9.65	9.59	9.53	9.58	9.78	9.79	9.78	9.75	9.73
Total	95.08	95.28	94.71	94.22	94.29	94.56	95.02	95.12	94.77	94.56
Si	5.575	5.564	5.587	5.567	5.589	5.563	5.576	5.583	5.565	5.563
Ti	0.281	0.280	0.273	0.280	0.281	0.326	0.32	0.314	0.315	0.303
Al^{IV}	2.425	2.436	2.413	2.433	2.411	2.437	2.424	2.417	2.435	2.437
Al^{VI}	0.486	0.481	0.480	0.482	0.475	0.367	0.391	0.403	0.396	0.401
Fe^{2+}	1.623	1.634	1.629	1.637	1.644	1.744	1.752	1.721	1.727	1.732
Mn	0.015	0.015	0.015	0.017	0.014	0.017	0.017	0.018	0.017	0.014
Mg	3.323	3.331	3.333	3.315	3.309	3.272	3.243	3.270	3.280	3.291
Ca	0.006	0.009	0.005	0.008	0.008	0.008	0.003	0	0.002	0.005
Na	0.072	0.063	0.093	0.085	0.076	0.070	0.067	0.07	0.07	0.07
K	1.837	1.828	1.827	1.828	1.836	1.880	1.873	1.866	1.867	1.867
Total	15.643	15.643	15.653	15.651	15.642	15.684	15.666	15.661	15.673	15.683
Fe/(Fe+Mg)	0.328	0.328	0.328	0.328	0.328	0.348	0.348	0.34	0.34	0.34
Mg/(Mg+Fe)	0.672	0.672	0.672	0.672	0.672	0.652	0.652	0.66	0.66	0.66

Number of ions on the basis of 22 oxygens. Total Fe is expressed as Fe^{2+}.

Table 4: Composition of the feldspar mineral from metamorphic sole rocks.

Rock Type	Amphibolite											
SAMPLE	M4 KF-1	M4 KF-2	M4 KF-3	M4 KF-4	M4 KF-5	M4 KF-6	M4 KF-7	M4 KF-8	M4 KF-9	M4 KF-10	M4 P-1	M4 P-2
SiO_2	63.61	64.61	63.48	60.28	64.02	64.52	61.59	62.84	62.33	63.08	56.45	56.54
Al_2O_3	18.64	18.51	18.81	18.06	18.52	18.54	17.41	17.82	17.46	18.23	27.54	27.69
FeO*	0	0	0.02	0.02	0.14	0.06	0.03	0.03	0.12	0.05	0.14	0.15
CaO	0.26	0	0.26	4.6	0.52	0.08	4.44	2.95	3.64	2.5	9.3	9.37
Na_2O	0.15	0.14	0.28	0.2	0.14	0.16	0.14	0.14	0.15	0.17	6.01	6.1
K_2O	16.46	16.63	16.23	14.27	16.34	16.75	14.71	15.44	15.07	15.65	0.08	0.07
TOTAL	99.13	99.9	99.08	97.46	99.68	100.11	98.32	99.22	98.87	99.68	99.52	99.92
Si	2.97	2.99	2.96	2.87	2.97	2.98	2.91	2.94	2.92	2.93	2.55	2.54
Al^{IV}	0.03	0.01	0.04	0.13	0.03	0.02	0.09	0.06	0.08	0.07	0.45	0.46
Al_{VI}	0.99	1.00	1.00	0.88	0.99	0.99	0.88	0.92	0.89	0.93	1.01	1.01
Fe^{2+}	0	0	0	0	0	0	0	0	0	0	0	0
Ca	0.01	0	0.01	0.23	0.03	0	0.22	0.15	0.18	0.12	0.45	0.45
Na	0.01	0.01	0.03	0.02	0.01	0.01	0.01	0.01	0.01	0.02	0.53	0.53
K	0.98	0.98	0.97	0.87	0.97	0.99	0.89	0.92	0.90	0.93	0	0
Total	5	5	5	5	5	5	5	5	5	5	5	5
Or	97.36	98.74	96.18	77.40	96.18	98.18	78.87	85.16	82.10	86.91	0.47	0.41
Ab	1.35	1.26	2.52	1.65	1.25	1.43	1.14	1.17	1.24	1.43	53.65	53.87
An	1.29	0	1.29	20.95	2.57	0.39	19.99	13.67	16.66	11.66	45.88	45.73

Number of ions the basis of 8 oxygens. Total Fe is expressed as FeO*.

Rock Type	Amphibolite												
SAMPLE	M4 P-3	M4 P-4	M4 P-5	M4 P-6	M4 P-7	M4 P-8	M4 P-9	M4 P-10	M4 P-11	M4 P-12	M4 P-13	M4 P-14	M4 P-15
SiO_2	58.06	57.6	57.69	55.79	55.62	56	56.34	55.81	56.15	56.16	56.04	56.04	56.11
Al_2O_3	26.52	26.63	26.66	27.9	28.1	27.73	27.68	28.01	27.92	28.02	27.98	28.02	27.77
FeO*	0.11	0.1	0.11	0.14	0.1	0.08	0.11	0.1	0.13	0.11	0.09	0.09	0.09
CaO	8	8.15	8.16	9.76	10.03	9.64	9.46	9.91	9.74	9.74	9.72	9.79	9.66
Na_2O	6.83	6.82	6.72	5.88	5.67	5.92	6.3	5.85	6.03	5.97	5.89	5.85	5.88
K_2O	0.05	0.06	0.04	0.06	0.07	0.06	0.06	0.08	0.08	0.09	0.08	0.09	0.07
TOTAL	99.57	99.36	99.38	99.53	99.59	99.43	99.95	99.78	100.05	100.09	99.8	99.88	99.61
Si	2.61	2.59	2.60	2.52	2.51	2.53	2.53	2.51	2.52	2.52	2.52	2.52	2.53
Al^{IV}	0.39	0.41	0.40	0.48	0.49	0.47	0.47	0.49	0.48	0.48	0.48	0.48	0.47
Al_{VI}	1.01	1.00	1.01	1.00	1.01	1.01	0.99	1.00	1.00	1.00	1.01	1.01	1.01
Fe^{2+}	0	0	0	0	0	0	0	0	0	0	0	0	0
Ca	0.39	0.39	0.39	0.47	0.49	0.47	0.45	0.48	0.47	0.47	0.47	0.47	0.47
Na	0.59	0.60	0.59	0.51	0.50	0.52	0.55	0.51	0.52	0.52	0.51	0.51	0.51
K	0	0	0	0	0	0	0	0	0	0.01	0	0.01	0
Total	5	5	5	5	5	5	5	5	5	5	5	5	5
Or	0.29	0.35	0.23	0.35	0.41	0.35	0.34	0.46	0.46	0.52	0.47	0.52	0.41
Ab	60.53	60.02	59.70	51.98	50.36	52.45	54.46	51.41	52.59	52.32	52.06	51.68	52.20
An	39.18	39.63	40.06	47.67	49.23	47.20	45.19	48.13	46.95	47.17	47.48	47.79	47.39

Number of ions the basis of 8 oxygens. Total Fe is expressed as FeO*.

U–Pb zircon ages determined for rocks in the study area overlap those previously calculated for the obduction and formation of ophiolite (Nurlu 2016; Nurlu et al. 2016). Even though the metamorphic sole rocks of the Meydan mélange have formed remarkable metamorphic rocks in the SAOB, the metamorphism and protolith of these rocks have not been documented. Zircons from the amphibolites of these sole rocks present mostly euhedral crystals and a smaller proportion of subhedral shapes, as observed in cathodoluminescence (CL) images (Fig. 5b,c). The examined zircons are mostly small to medium in size (90–270 μm). The zoning types revealed in the CL images include growth, convolute, sector, and, in particular, oscillatory. The internal structure includes pyramidal, stubby prismatic, and prismatic shapes with crystal facets observed in some grains. The Cl images of zircons from amphibolites clearly show crystals with oscillatory zoning and prismatic internal growth, which are consistent characteristics of magmatic zircons. Oscillatory and sector zoning has been slightly obliterated, with luminescent patches on some zircons, indicating some degree of recrystallization. The Supplementary Table S2 provides analytical data and estimated concordia diagrams for both dated samples (Fig. 5a). Six zircons from the metamorphic sole rock (MG-2) in the Meydan mélange yielded ages of 83.8±2.0 to 91.6±1.3 Ma (2σ) with a concordia of 85.4±0.93 Ma (Fig. 5a). Sample number MG-1 includes 31 zircons, yielding ages of 78.9±1.7 to 89.9±2.2 Ma (2σ) with a concordia age of 81.45±0.69 Ma (Fig. 5c). Previous research (Nurlu et al. 2016; Nurlu 2016) suggests that the Meydan ophiolite formed between 79.8±1.1 Ma and 83.1±1.5 Ma.

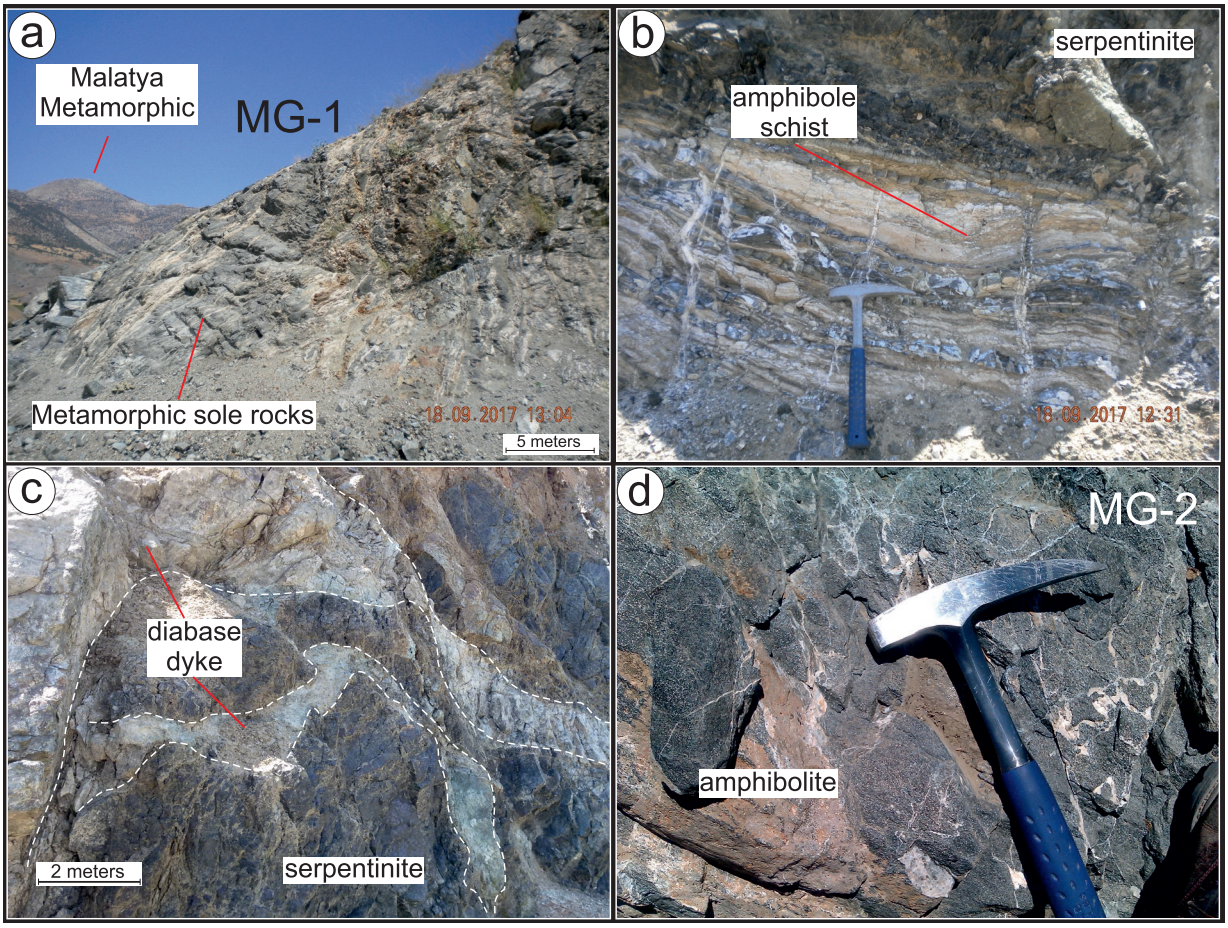

Fig. 3. Detailed field relation of the amphibolites and mafic dikes of Meydan mélange.

Geochemistry

Mineral chemistry

Two amphibolite samples were selected to examine the mineral chemistry, particularly that of the amphiboles. Two groups of amphiboles were detected. Group I samples are represented by magnesio-hornblende, and Group II samples are characterized by ferro-actinolite, indicating a metamorphic peak and a late event, respectively (Fig. 6a; Table 2a–c). An examination of the amphiboles from the metamorphic sole rocks indicated a calcic amphibole content in accordance with the classification of Hawthorne et al. (2012). The representative Group I (Mg–Hb) amphiboles are defined by SiO_2=44.09–50.54 %, TiO_2=0.52–0.87 %, Al_2O_3=5.94–11.58 %, FeO=10.34–13.48 %, MgO=11.55–15.78 %, and K_2O=0.25–0.56 %. Group II (Fe–Act) amphiboles are characterized by SiO_2=52.51–53.92 %, TiO_2=0–0.03 %, Al_2O_3=0.25–0.54 %, FeO=18.67–21.8 %, MgO=8.39–10.94 %, and K_2O=0.01–0.25 %. A wide range of X_{Mg} (Mg/Mg+Fe^{2+}) values were observed, although most were in the range of 0.63–0.77 (Table 2). The amphiboles exhibited Mg depletion as well as decreasing Al_2O_3 and Fe^{2+} but increasing SiO_2 values. The calcic amphiboles in the metamorphic sole rocks were found to have ferro-actinolite to magnesio-hornblende compositions (Fig. 5a). Inverse thermobarometry was conducted on the basis of the amphibole–plagioclase and Ti-in-hornblende compositions (Johnson & Rutherford 1989; Holland & Blundy 1994), whereas the amphibole structural formulae were calculated by using an ACES2013 Excel spreadsheet (Locock 2014). All the amphibole values, given in Table 2a,b, were calculated by using the Excel spreadsheet for the Al-in-hornblende geobarometry (Anderson et al. 2008) and Pl–Hbl thermometry; the calculation equation was $0.5+(0.331\times Altot)+[0.995\times(Al_{tot}\times Al_{tot})]$ (Holland & Blundy 1994; Anderson et al. 2008). The results provided by the inverse geothermobarometry models were interpreted using the ISOPLOT 4.15 Excel add-in (Ludwig 2003) and were used for weighted average calculations of the T–P conditions. The obtained amphibole data were expressed using the statistical approach suggested by Calzolari et al. (2018). For Group I amphiboles from the amphibolites, the inverse geothermobarometry models yielded a weighted average value of 2.38±0.33 kbar (95 % conf., MSWD=1.9), with a weighted average value of 0.52±0.011 kbar (95 % conf., MSWD=2.1). For Group II amphiboles from the amphibolites, the temperatures ranged from 613±25 °C to 660±40 °C with a weighted mean value of 630±16 °C (95 % conf.,

MSWD=2.3). For Group II amphiboles, the thermometry models yielded a weighted mean value of 547±35 °C, varying between 545±38 °C and 549±40 °C (95 % conf., MSWD=1.7). Best (1982) suggested that on an Al_2O_3, CaO, and FeO+MgO (ACF) diagram, the amphibolite facies of metamorphic rocks and amphibolitic rocks principally fall in the hornblende and biotite zone of the mafic rocks (Fig. 7a). The tobermorite, prehnite and pumpellyite analyses fall outside both the greenschist and actinolite schist sub-areas (Fig. 7a). In addition to Al-in-hornblende geobarometer modelling, the semi-quantitative geobarometer presented by Brown (1977) was used to determine the pressure evolution of the amphiboles from

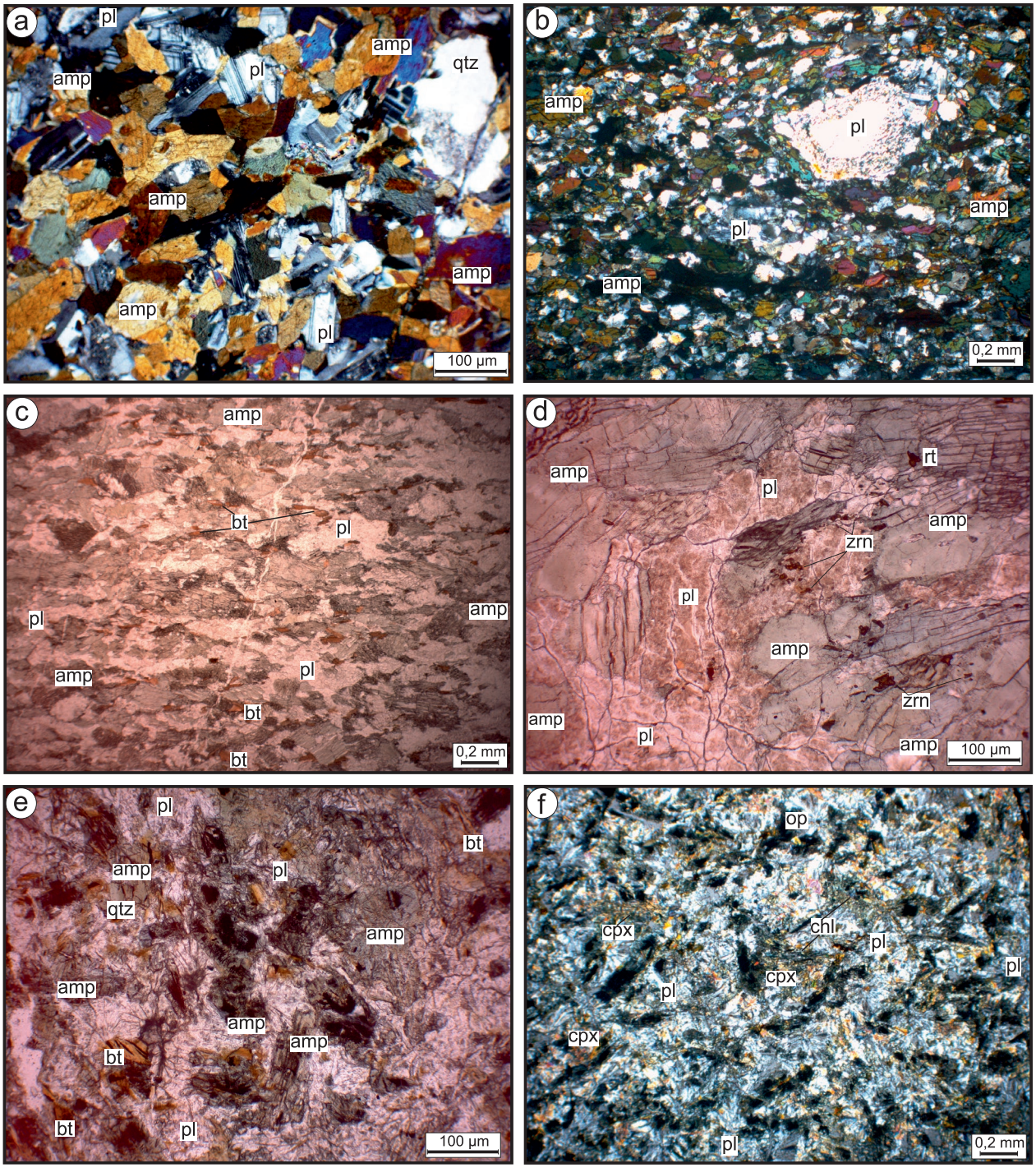

Fig. 4. Petrographic characteristics of Meydan ophiolite and Meydan Mélange and amphibolites within the Helete and Meydan region. **A** — Photomicrograph of the amphibolites; **B** — Porphyroblastic texture of the actinolite schist; **C** — General view of the biotite amphibole schist; **D** — Nematoblastic texture of amphibole schist; **D/E** — Photomicrographs of mafic dikes. Mineral abbreviations: amp — amphibole; pl — plagioclase, qtz — quartz; rt — rutile; bt — biotite; zrn — zircon.

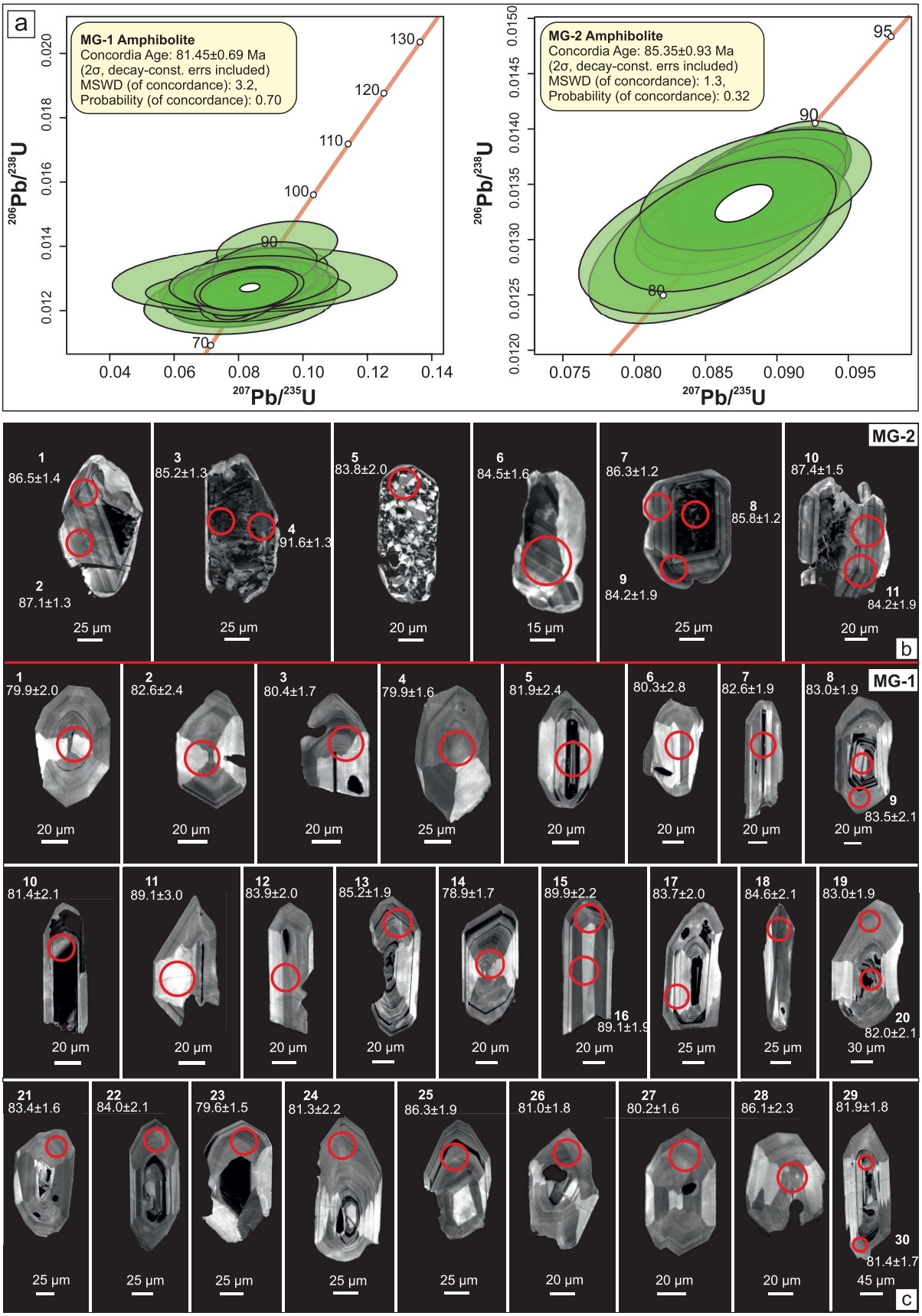

Fig. 5. **A** — Plots of U–Pb zircon ages of the amphibolites (MG1, MG2). See text for explanation. **B** — Cathodoluminescence images of zircons from the amphibolites (MG2). **C** — Cathodoluminescence images of zircons from the amphibolites (MG1).

the metamorphic sole rocks. The reading was less than 0.5 GPa. The pressure for the metamorphic sole rocks, calculated from the ratios of the Na^{M4}–Al^{IV} apfu numbers from the amphiboles, was 2.5–5 kbar (Fig. 7b). These two geobarometry models presented reliable and compatible results.

The studied pumpellyite displayed considerable compositional variations in the $Al_{(total)}$–Fe–Mg (AFM) diagram (Fig. 6b). According to the AFM content, all the pumpellyite compositions indicate subduction-related settings such as the actinolite–pumpellyite facies of California (Supplementary Table S3; Coombs et al. 1976; Liou & Ernst 1979).

The Al–Si–M^{2+} triangular diagram discriminates sidorophyllite, muscovite, eastonite, phengite, and biotite (Deer et al. 1992), which illustrates fundamental variations in the mica content. The biotite from the metamorphic sole rocks of the Meydan mélange plotted relatively high M^{2+} akin to that for phlogopite (Table 3; Fig. 6c). The examined micas from these sole rocks have been defined as biotites, based on the Al–Si–M^{2+} triangular diagram (Fig. 6b). The Si composition of the biotite in the Meydan mélange ranges from 5.59 to 5.56 apfu and does not display zonation. The biotite is defined by TiO_2 in the range of 2.43–2.88 apfu and X_{Mg} (Mg/Mg+Fe) ratios of 0.65–0.66 apfu. In the An–Ab–Or ternary classification diagram suggested by Leake & Woolley Arps (1997), the analysed feldspars include andesine, labradorite, orthoclase, and two feldspar compositions (Fig. 6d; Table 4).

The tobermorite group and zeolite were found only in the upper section of the metamorphic sole rocks. Zeolite was observed very rarely in the amphibolites; its crystals are associated solely with ferro-actinolite and tobermorite group minerals, which formed colourless, glassy crystals 3–5 mm in length. The analysed zeolite contains elements in the following ranges: 47.28–49.08 % SiO_2, 29.63–31.44 % Al_2O_3, 2.15–5.16 % CaO, and 12.27–14.2 % Na_2O.

Whole-rock geochemical features

The whole-rock major and trace element contents of the mafic dikes and metamorphic sole rocks from the Meydan mélange are listed in Table 1. High field strength elements

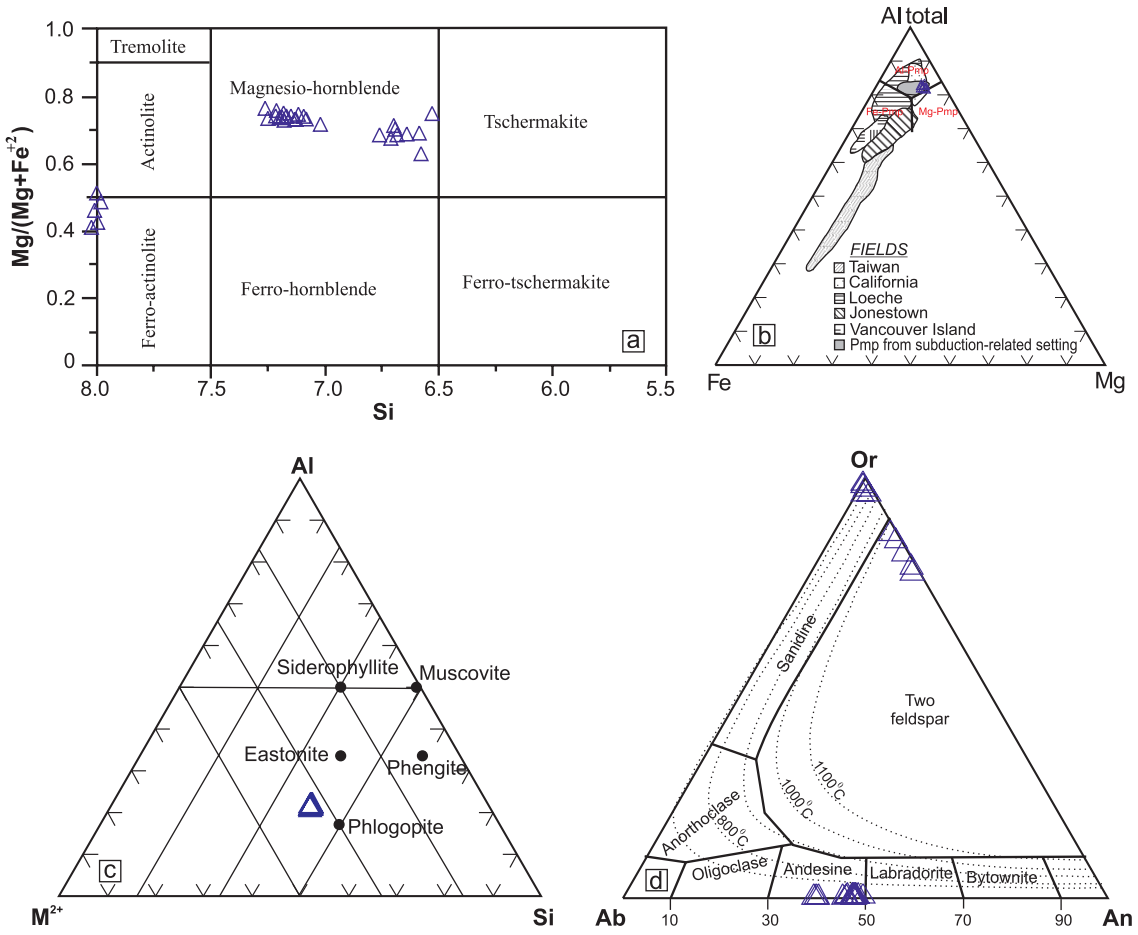

Fig. 6. A — The chemical composition of amphiboles in the metamorphic sole rocks of the Meydan mélange. **B** — Chemical compositions of the examined biotites from the metamorphic sole rocks on a ternary diagram of Al–Si–M^{2+}. **C**— Chemical compositions of feldspars from the metamorphic sole rocks of Meydan mélange (after Leake & Woolley Arps 1997). **D** — Contents of the pumpellyite on Al–Fe–Mg discrimination diagram (apfu) where Al=total Al. The discrimination layout of Passaglia and Gottardi (1973) and the fields from distinct metamorphic territories after Coombs et al. (1976) and Liou & Ernst (1979) are indicated for comparison and (grey area) of pumpellyite defined in other subduction-related settings (Nishimura et al. 2000, Potel et al. 2002, Krenn et al. 2004) have also been included.

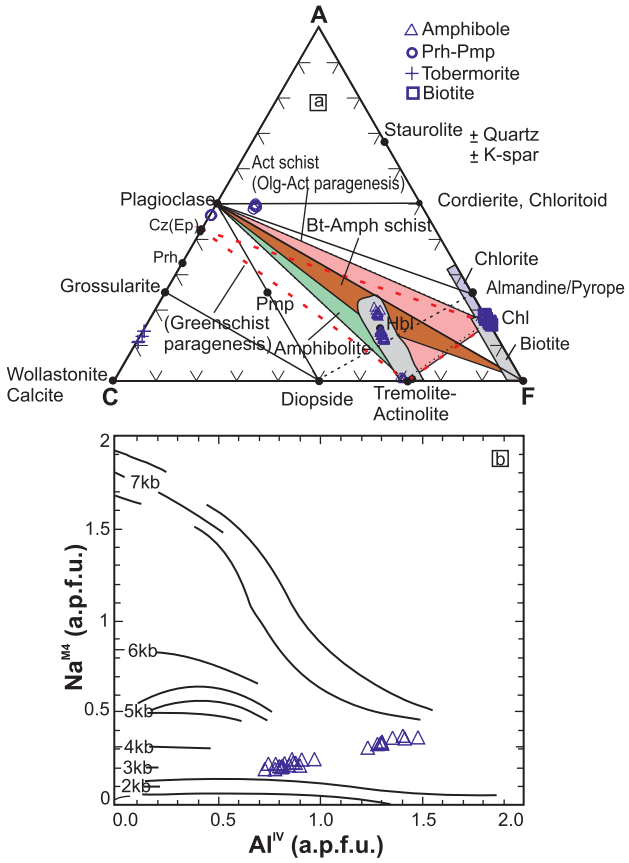

Fig. 7. A — Mineral assemblages of the amphibolites from Meydan Mélanges are shown in the ACF diagram (Best 1982). $A=Al_2O_3+Fe_2O_3\pm(Na_2O+K_2O)$; $C=CaO-3{,}3P_2O_5$; $F=FeO+MgO+MnO$. **B** — Comparison of Na^{M4} and Al^{IV} positions for amphibole from metamorphic sole rocks of the Meydan mélange (after Brown 1977).

(HFSEs) are mostly immobile and are typically resistant to hydrothermal alteration and metasomatism. Thus, HFSE have been selected and applied to discrimination diagrams for the classification of the amphibolites and mafic dikes. The discrimination diagrams of Pearce & Cann (1973) and Winchester & Floyd (1977) were used to constrain the provenance of the dikes and the protolith of the metamorphic rocks according to their proportions of HFSEs and rare earth elements (REEs). On the Zr/Ti versus Nb/Y diagram (Fig. 8a), the metamorphic rocks commonly plotted in the field of tholeiitic basalt, whereas the mafic dikes plotted in the basaltic andesite field, having low concentrations of Ti (2577.85–4676.10 ppm), Nb/Y (0.03–0.13 ppm), Zr (29.3–44.5 ppm), and P_2O_5 (0.04–0.09 wt. %; Fig. 8a). The amphibolites and amphibole schists of the metamorphic sole rock and mafic diabase dikes suggest a basaltic andesite protolith (Fig. 8a). The amphibolites and mafic dikes of the Meydan mélange are tholeiitic in nature and are similar to the isolated dikes and amphibolites of the inner Tauride suture zone and Kömürhan ophiolites (Fig. 8b). They are depleted in Nb and enriched in large-ion lithophile elements (LILEs) such as Cs, Rb, Ba, and K, and they exhibit flat patterns of heavy rare earth elements (HREEs), in comparison with those of normal mid-ocean ridge basalt (N-MORB; Fig. 9a). The amphibolites display multi-element patterns akin to the suggested tholeiitic amphibolites and isolated dikes beneath the inner Tauride suture zone ophiolites (Fig. 9a). The relative enrichment in Th, compared with the Nb depletion of the amphibolites in the metamorphic sole rocks and mafic diabase dikes, indicate that the corresponding magmas were generated in an SSZ environment (Pearce et al. 1984). The chondrite-normalized REE patterns of the Meydan region amphibolites and mafic dikes are

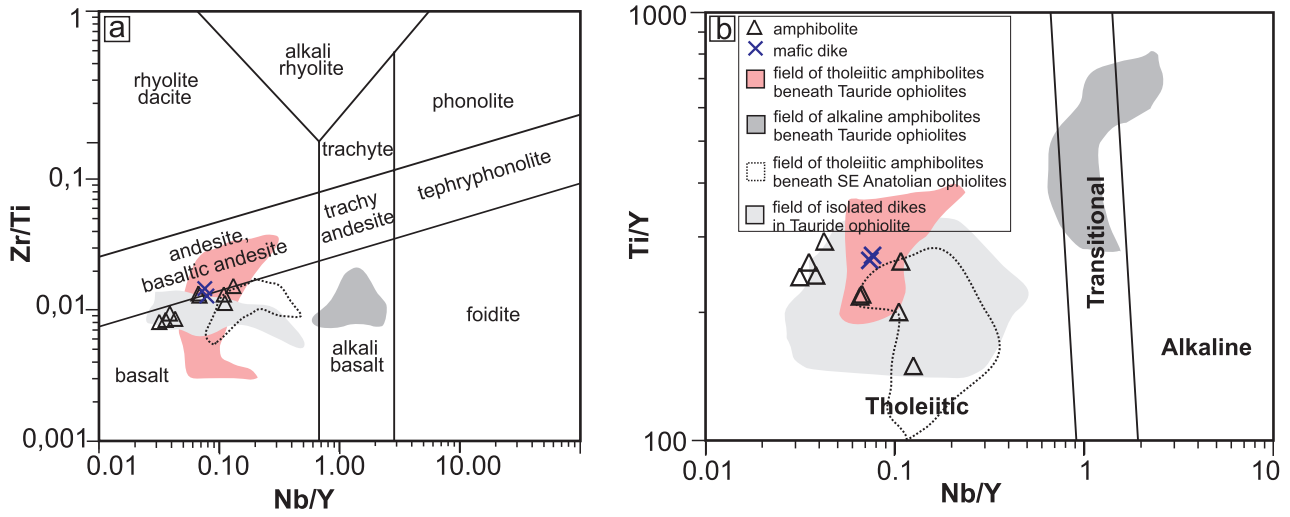

Fig. 8. A — Zr/Ti versus Nb/Y diagram illustrating potential protoliths for amphibolites and mafic dikes from the Meydan mélange (Winchester & Floyd 1977). Field of the amphibolites and isolated dikes are taken from Lytwyn & Casey 1995; Parlak et al. 1995; Parlak & Delaloye 1996; Çelik & Delaloye 2003. **B** — Nb/Y against Ti/Y diagram for the amphibolites and mafic dikes of the Meydan mélange (after Pearce 1982). Field of the amphibolites and isolated dikes in Tauride ophiolites are taken from Lytwyn & Casey 1995; Parlak et al. 1995; Parlak & Delaloye 1996; Çelik & Delaloye 2003 and field of the amphibolites beneath SE Anatolian ophiolite are taken from Rızaoğlu et al. 2006.

presented in Fig. 9b (Sun & McDonough 1989). The mafic dikes exhibit slight LREE enrichment and relatively depleted REE patterns, compared to those in the mafic dikes in the Tauride suture zone ophiolites (La_N/Yb_N=1.06–1.27; Lytwyn & Casey 1995; Parlak et al. 1995; Parlak & Delaloye 1996; Çelik & Delaloye 2003; Rızaoğlu et al. 2006). The amphibolites and amphibole schists of the Meydan mélange present the flat-type REE patterns (La_N/Yb_N=0.94–2.16) of basaltic rocks formed by supra-subduction processes (Sun & McDonough 1989). These REE patterns are present in related metamorphic sole rocks that lie beneath the Tauride and SAOB and suggest that they were formed by basaltic volcanism in an IAT setting (Fig. 9).

Mullen (1983) presented a MnO–TiO_2–P_2O_5 triangle diagram that discriminates IAT, MORB, OIT, and CAB subfields and examined a plot of amphibolites and mafic dikes in the IAT basalt fields (Fig. 10a). The clear arc signature of the amphibolites and mafic dikes was observed in the Zr versus Zr/Y diagram (Figure 10b) (after Shervais 1982). The V versus Ti/1000 discrimination diagram suggests three tectonomagmatic subfields, and the amphibolites and mafic dikes of the Meydan mélange plotted in the IAT subfield (Fig. 10c) (after Pearce & Norry 1979). The Ce/Sm versus Sm/Yb values used to define the mantle source regions for the mafic dikes and amphibolites indicate that these rocks were produced from the melting of a MORB-like mantle with relatively low Ce/Sm and Sm/Yb values, with ratios comparable to those of the tholeiitic amphibolites beneath the Tauride belt ophiolites (Fig. 11a). To examine the processes involved in the evolution of the metamorphic sole rocks and the mafic dikes from the Meydan mélange, estimates based on mixing, assimilation–fractional crystallization (AFC), and fractional crystallization (FC) models (Ersoy 2013) were made for the amphibolites and diabase dikes, yielding ~35 % hornblende, ~5 % clinopyroxene, and ~60 % plagioclase. The data showed that a single evolutionary process is highly unlikely for the metamorphic sole rocks and mafic dikes (Fig. 11b,d). The Zr/Nb versus Ti/Nb ratios of the amphibolites and mafic dikes indicate that these rocks are similar to N-MORB (Fig. 11b).

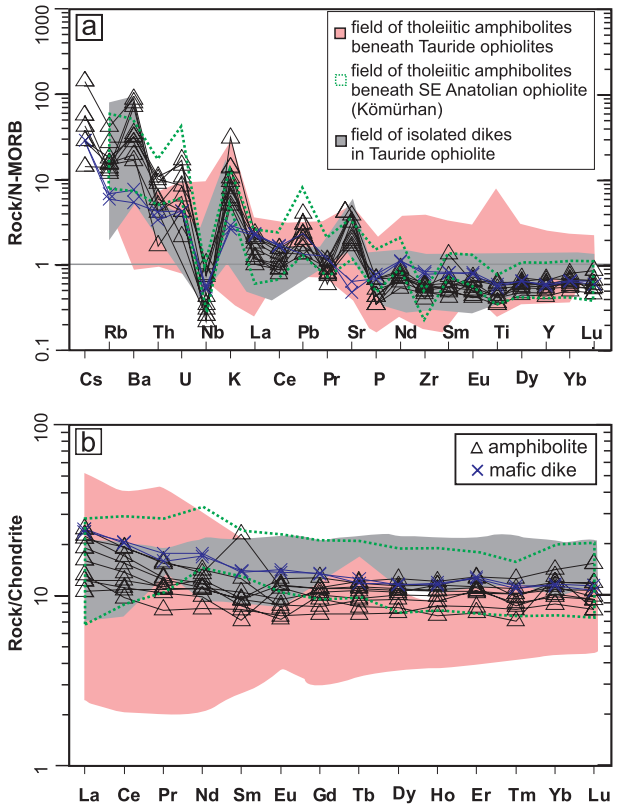

Fig. 9. A — N-MORB-normalized trace elements are plotted for the amphibolites and mafic dikes from the metamorphic sole rocks of the Meydan mélange. **B** — Chondrite-normalized REE patterns of the amphibolites and mafic dikes from the metamorphic sole rocks of the Meydan mélange (normalizing values are taken from Sun & McDonough 1989). Field of the amphibolites and isolated dikes in Tauride ophiolites are taken from Lytwyn & Casey 1995; Parlak et al. 1995; Parlak & Delaloye 1996; Çelik & Delaloye 2003 and Field of the amphibolites beneath SE Anatolian ophiolite are taken from Rızaoğlu et al. 2006.

Discussion

The SAOB is a crucial area for researching developments in an ophiolite setting throughout the vast Alpine–Himalayan mountain chain. The Neo-Tethyan reconstruction for the Late Cretaceous epoch interval of the eastern Mediterranean region proposes three distinct branches of ocean basins divided by platform carbonates and continental fragments. From south to north, these include the southern Neo-Tethys, Inner Tauride Ocean, and northern Neo-Tethys (Şengör & Yılmaz 1981). The Cretaceous ophiolites and ophiolite-related rocks that form the southern part of the Tauride platform in southern Anatolia were emplaced southward onto the northern side of the Arabian continent and were reproduced from the southern Neo-Tethys (Fig. 1; Robertson et al. 2007). The metamorphic rocks from the Late Cretaceous Meydan mélange in South-East Turkey are highly foliated, showing minerals with parallel orientations. This suggests that the inner geochemistry and structural properties of this ophiolite may provide evidence of seafloor spreading tectonics during the early phases of basin sealing in the southern Neo-Tethys and a supra-subduction setting (Fig. 1; Şengör & Yılmaz 1981; Yılmaz et al. 1993). Metamorphism occurred throughout the intra-oceanic subduction in the Neo-Tethyan oceanic basin (Lytwyn & Casey 1995; Parlak 1996; Dilek et al. 1999; Çelik & Delaloye 2003; Çelik et al. 2004; Rızaoğlu et al. 2006). The Meydan mélange is composed mostly of metamorphic sole rocks (e.g., amphibolite, biotite schist), marble, serpentinized peridotites, spilite, calc–schist, and granite, as identified in samples obtained near Savran village in the SAOB (Nurlu et al. 2016). It is widely accepted that metamorphic sole rocks are formed at the bases of mantle tectonites for the following reasons: i) The serpentinized harzburgite from the mantle tectonites and metamorphic sole rocks of the Meydan mélange show intrusions by the same unmetamorphosed mafic diabase dikes (Fig. 12b);

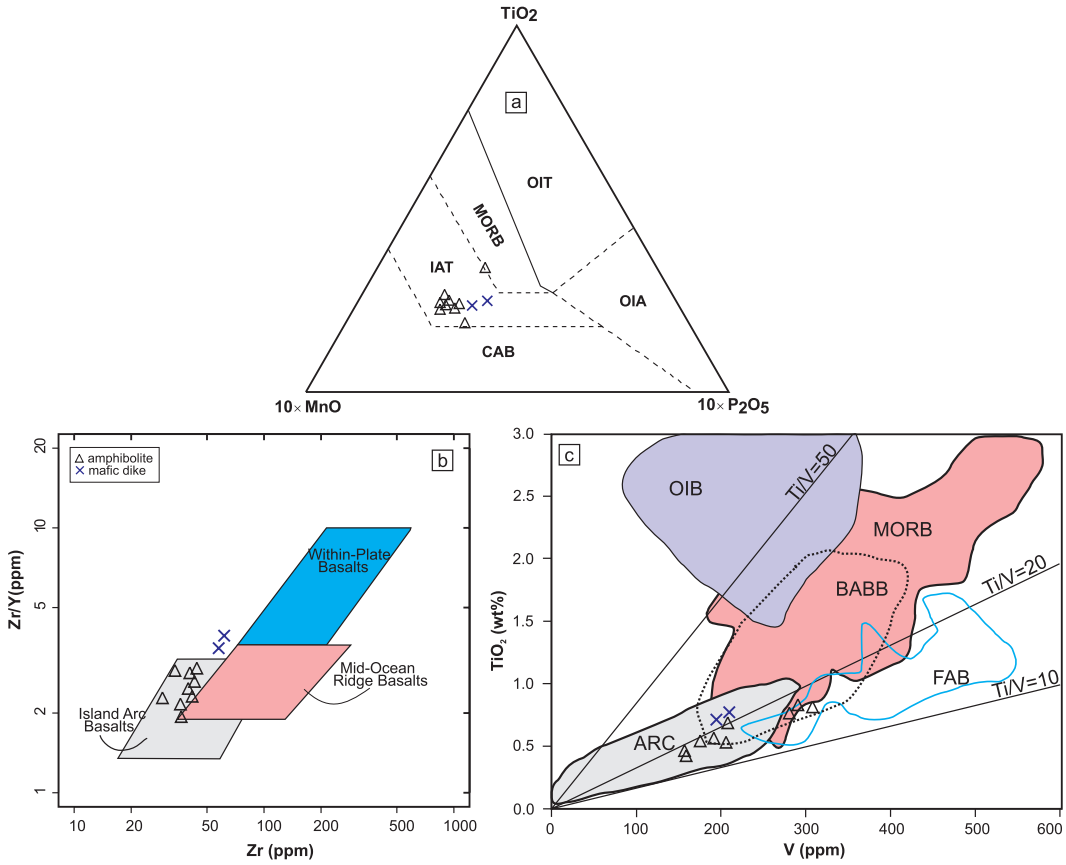

Fig. 10. A — MnO–TiO_2–P_2O_5 triangle diagram (Mullen 1983). **B** — Zr/Y versus Zr tectonomagmatic discrimination diagram after Pearce & Norry (1979). **C** — V versus Ti illustrating discrimination diagram of amphibolites and mafic dikes after Shervais (1982) and OIB, ARC, BABB, MORB, FAB fields are after Rossetti et al. (2017).

ii) The serpentinized peridotites occur together with the metamorphic sole rocks; and iii) the foliations observed in both units are in parallel arrangement. The genesis of the metamorphic sole rocks can be interpreted within the wider context of early supra-subduction evolution and its participation in the ophiolite development. The diverse metamorphic circumstances caused metamorphism to occur in the cold oceanic lithosphere, which was then subducted at the base of the hot oceanic lithosphere through intra-oceanic supra-subduction events (Malpas 1979; Spray 1984). The amphibolites from the metamorphic sole rocks provide crucial information regarding the tectonic setting of the subducted oceanic lithosphere as well as the P–T conditions and age of the metamorphism (Malpas 1979; Spray 1984; Hacker 1991; Çelik & Delaloye 2003, 2006; Çelik 2007, 2008; Wakabayashi et al. 2010). The metamorphic sole rocks are well preserved in the Meydan mélange, both to the south-east of Savran village and in the town of Helete. Several researchers have suggested the presence of metamorphic sole rocks beneath the Neo-Tethyan ophiolites in locations such as Pınarbaşı, Mersin, Divriği, and Kömürhan in Turkey and Semail in Oman (Searle & Cox 2002; Çelik & Delaloye 2003; Vergili & Parlak 2005; Çelik et al. 2004; Parlak et al. 2005; Kakar & Mahmood 2015; Roberts et al. 2016).

Geodynamic environment and depth of metamorphic sole rocks

The flat to LREE-enriched signature is generally attributed to mantle enrichment by components related to supra-subduction (Floyd et al. 1991). The IATs have characteristically flat to LREE-enriched signatures (Pearce 1982), which are also present in the SSZ ophiolites of the Taurides and SAOB (Pearce et al. 1984; Yalınız et al. 1996; Parlak et al. 2000; Rızaoğlu et al. 2006). The flat-type REE patterns presented in the studied rocks are representative of SSZ-setting ophiolites in Turkey (Parlak 1996; Yalınız et al. 1996, 2000; Parlak et al. 2000, 2004; Parlak & Robertson 2004) and IAT series rocks (Jakes & Gill 1970). The REE characteristics of magma are affected by distinct magmatic processes, which can ultimately cause consistent fractionation in the REEs. The REEs are highly useful in petrological investigations of basaltic/gabbroic rocks because they are relatively immobile even when subjected to a high/moderate degree of metamorphism and weathering, and they occur in a coherent cluster of incompatible elements (Hanson 1980; Bernard et al. 1985). The REEs are insensitive to crystal fractionation, except for Eu, and they tend to concentrate in the melt. Therefore, they are significant indicators of the source of mafic rocks, particularly basalt.

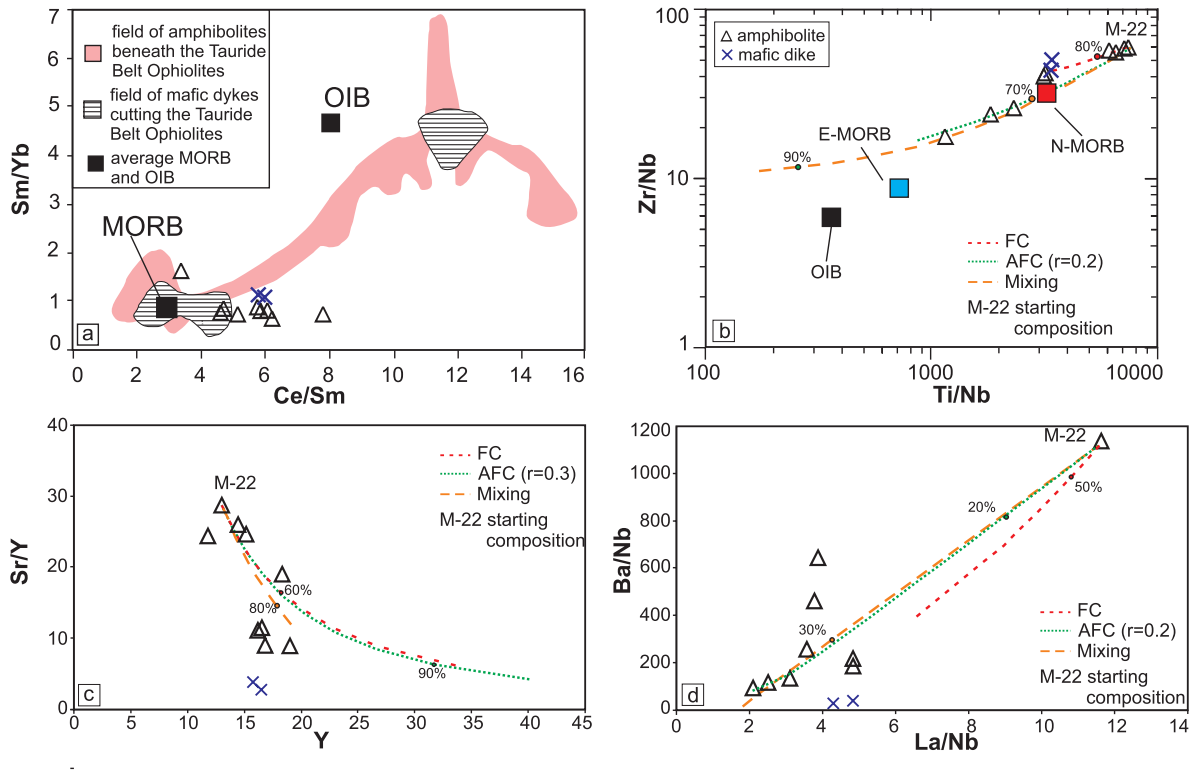

Fig. 11. A — Ce/Sm vs Sm/Yb discrimination diagram, after Pearce (1982), defining source properties for the mafic dikes and amphibolites Fields of MORB and OIB are taken from Harms et al. (1997). **B** — Zr/Nb versus Ti/Nb diagram preferring distinct magma sources for origins of metamorphic sole rocks and mafic dikes and showing FC-AFC and mixing models (Ersoy 2013). Fields of amphibolites and isolated dikes from Turide ophiolites are from Lytwyn & Casey (1995), Parlak et al. (1995, 2006), Çelik & Delaloye (2003), Vergili & Parlak (2005). **C** — Sr/Y versus Y and **D** — Ba/Nb versus La/Nb diagrams presenting FC-AFC and mixing models for amphibolites and mafic dikes (Ersoy 2013).

Most of the amphibolite samples are characterized by high Ti/Nb values, which is attributed to the presence of rutile (Fig. 4d–Fig. 11b). In addition, in the Zr/Nb versus Ti/Nb, Ba/Nb versus La/Nb, and Sr/Y versus Y diagrams (Fig. 11b,d) and in calculations using an M-22 sample as the starting composition, the amphibolites and mafic dikes clearly indicate a mixing–AFC trend with remarkable contribution from crustal sources in the formation of the M-22 amphibolite, both as rock-contaminants and crustal melt. The examined amphibolites and mafic dikes display geochemical characteristics indicative of this interaction, such as broadly variable Ba/Nb values ranging from 26.15 to 1124.01 and low La/Nb values ranging from 2.13 to 11.6 (Fig. 11d). In addition, the Ce/Pb values, with an average of 4.92, might also represent contamination of the amphibolite and mafic dike samples by a continental-crust component because the average Ce/Pb ratio of the continental crust is 3.9 (Table 1; Shimizu & Arculus 1975; Pearce 1983; Rudnick & Fountain 1995; Rudnick & Gao 2003). Rutile is associated with relative Ti enrichment rather than Nb depletion. Moreover, rutile forms under relatively high-temperature or high-pressure conditions and occurs primarily in high-grade metamorphic rocks (Ernst & Liu 1998; Meinhold 2010). However, several researchers have determined that rutile can also occur occasionally in phyllite and greenschist, which are low-grade metamorphic rocks (Luvizotto & Zack 2009; Luvizotto et al. 2009). Most of the accepted models support the explanation that the rutile in metamorphic rocks occurs from the replacement of Fe–Ti oxides, titanite, and high-Ti biotite throughout prograde to peak metamorphic phases (Zack et al. 2002; Luvizotto & Zack 2009; Luvizotto et al. 2009; John et al. 2011). On the contrary, however, rutile is completely or partially converted into the previously discussed Ti-rich phases, throughout the retrogression, depending on decreases in pressure and temperature. The lineal mineralogical occurrence of the latest process involves titanite or Fe–Ti oxide rims around rutiles in amphibolites, eclogites, and similar lithologies (Yang 2004; Lucassen et al. 2010; Cruz-Uribe et al. 2014).

As suggested by Rızaoğlu et al. (2006), the metamorphic sole rocks from the Kömürhan ophiolite in South-East Turkey are mostly basaltic protoliths from solely IAT rocks and are metamorphosed equivalents of tholeiitic basalts with very similar geochemistry (Fig. 10). The amphibolites of the metamorphic sole rocks and mafic diabase dikes of the Meydan mélange are tholeiitic in character, with Nb/Y=0.032–0.131. The tectonomagmatic discrimination diagrams, REE patterns, and multi-element patterns indicate that the protolith of the metamorphic sole rocks is close to an IAT. Moreover, the mineral chemistry data from the pumpellyite confirm the character of the SSZ setting.

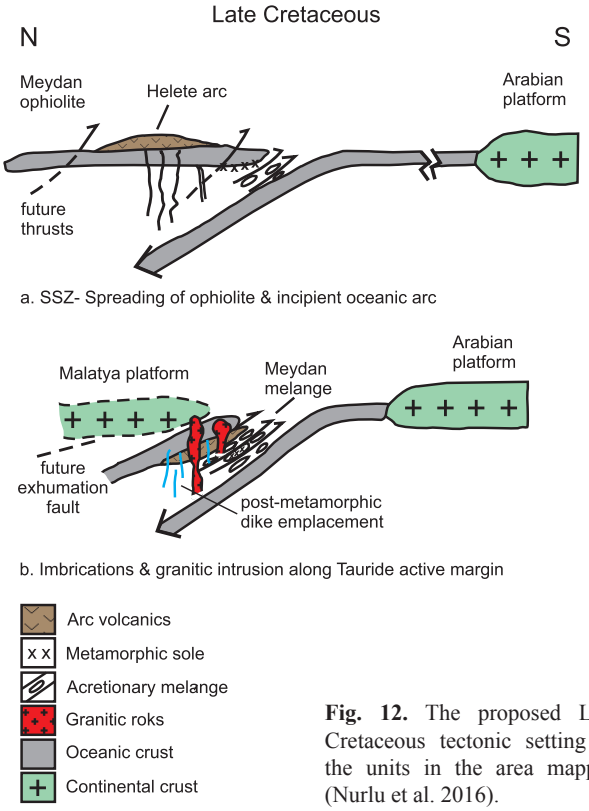

Fig. 12. The proposed Late Cretaceous tectonic setting of the units in the area mapped (Nurlu et al. 2016).

Temperature and pressure were calculated on the basis of the hornblende–plagioclase (Anderson 1996) geothermobarometry. In addition, a guideline was provided to define the pressure of the metamorphism and thermobaric environment of the metamorphic sole rocks in the amphibole calculations (Lucci et al. 2018). The calculated geobarometric pressure for the amphibolites had a weighted average value of 2.38±0.33 kb, varying between 1.84 and 5.32±0.5 kb, for the magnesio-hornblende (Group I), and a weighted average value of 0.52±0.01 kb, varying between 0.51 and 0.53±0.5 kb, for the ferro-actinolite (Group II). The calculated metasomatism depths were approximately 9 km based on an average crustal specific gravity of 3.0 g/cm^3. The amphibolites of the region near Helete and Savran villages showed temperatures ranging from 614 °C to 660 °C±40 °C, with a weighted mean value of 630 °C±16 °C. The evaluated structure discordances suggest that the overall amphibolite section has been overprinted by prehnite (pumpellyite) and greenschist facies minerals throughout the subsequent retrogression. The predominant retrograde phases in the metamorphic soles include acicular ferro-actinolite, albite, prehnite, and pumpellyite. Actinolites (secondary amphibole) occur at the expense of hornblende (primary amphibole), whereas prehnite and Al-pumpellyite replace the plagioclase.

The actinolites are believed to have formed through retrograde metamorphism of Fe-rich minerals such as clinopyroxene and olivine. The presence of hornblende in amphibolite and biotite-amphibole schist rock types indicates that the temperature is higher than that required for the reaction An+Act+Chl→Hbl, thereby resulting in a higher grade than that of the actinolite schist. The amphiboles showed two distinct total Al clusters of which the total observed Al compositions were in the ranges of 1.01–2.04 apfu and 0.045–0.344 apfu, respectively. The Al-rich amphiboles are mostly magnesio-hornblende, whereas the Al-poor amphiboles are mainly ferro-actinolite (Table 2a–c).

The zircons from the metamorphic rocks largely lack oscillatory zoning (e.g., Kröner et al. 1987). Alteration patterns that could be attributed to metamorphism are recognizable in the zircon photographs. These patterns represent extremely luminescent domains resulting from alteration of primary growth structures such as growth banding and sector zoning that truncate the primary zoning in almost all grains (Fig. 5c; e.g., Vavra et al. 1999). The Th/U ratios obtained from the zircon ages range from 0.71 to 0.09, with almost all above 0.1, and plotted mostly in the magmatic and intermediate areas. This also confirms a magmatic protolith (Teipel et al. 2004). Additionally, these Th/U ratios and zircon textures imply the protolith age of the amphibolite and prove its common provenance with the Meydan ophiolite. However, the pattern of alteration does not appear to be associated with the primary textures and is represented solely by luminescent crystal rims below corroded crystal surfaces (Fig. 5b: 1, 3, 6, 11; e.g., Vavra et al. 1999). Metabasite rocks show prismatic internal growth bands and euhedral, occasionally un-recrystallized, magmatic domains that hold the original oscillatory zoning in metamorphic zircons (e.g., Vavra et al. 1996). These domains are considered to represent the unaltered magmatic zircon of the protolith (Vavra et al. 1996; Watson 1996). Based on the evidence of almost all Th/U ratios above 0.1 as well as the zircon textures and calculated temperatures of amphibolites fitting subsolidus conditions (~ 630 °C), it is believed that the ages of the dated zircons are inherited from the pristine basaltic zircons rather than the metamorphism. The U–Pb zircon ages for the protolith of the metamorphic sole rocks of the Meydan ophiolite reveal that magmatic precursor and/or metamorphism occurred during or prior to the formation of the ophiolite crust and were later juxtaposed with the base of the Meydan ophiolite. This finding has not been reported thus far. It is widely accepted that the formation of the metamorphic sole rocks beneath the Neo-Tethyan ophiolites, particularly the Tauride and south-east Anatolian ophiolites, depended on the initiation of the subduction and the emplacement process (Vergili & Parlak 2005; Çelik 2007, 2008). Nurlu (2016) reported that the volcanic rocks of Meydan ophiolite show a bimodality composition from basic and acidic features and are cut by leucocratic rocks, particularly granite and granodiorite. According to the U–Pb ion probe dating of zircons in these rocks, the ages of the leucocratic rocks range from 87.9±1.5 Ma to 85.9±1.4 Ma.

These volcanic rocks were geochemically derived from tholeiitic magma and were formed in a Late Cretaceous SSZ. Potential mantle sources might be indicated by the asthenosphere metasomatized by subduction-related melts/fluids or by the metasomatized continental lithospheric mantle. The metamorphism of the IAT-type basalt and basaltic andesite occurred

when the amphibolites of the metamorphic sole rocks were separated from the upper section of the subducted oceanic crust and were underplated. The precise U–Pb zircon age data obtained from the protolith of the metamorphic sole rocks are compatible with the ages obtained from the gabbroic rocks of Meydan ophiolite (Nurlu 2016; Nurlu et al. 2016).

Conclusions

From the results of this analysis and the subsequent discussion, the following conclusions were drawn.

- Sub-ophiolitic amphibolite facies are created as blocks of metamorphic rock and form the sole of the ophiolite segments in the ophiolite-related mélange zone beneath the Meydan ophiolite. The metamorphic sole rocks are composed of four lithologies: biotite amphibole schist, prehnite–pumpellyite–amphibole schist, actinolite schist, and amphibolite.
- The metamorphism of an IAT-type basalt and basaltic andesite protolith formed the amphibolites of the metamorphic sole rocks throughout a period of intra-oceanic thrusting and subduction. These volcanic rocks are likely to have been separated from the upper part of the Meydan ophiolite and were subsequently metamorphosed and underplated.
- The analysed magnesio-hornblende from the amphibolites in the metamorphic sole rocks experienced estimated pressures of 1.84–5.32 kb with a weighted mean value of 2.38±0.33 kb at an approximate depth of 9 km as well as temperatures of 613–660 °C during the metamorphism with a weighted average value of 630 °C±16 °C.
- These new, high-precision U–Pb data provide insight into the source of the amphibolites of the Meydan mélange. The protolith of these amphibolites in the Helete region includes two typical types of metamorphic sole rocks of the SAOB and the Inner Tauride belt. These are mafic rocks of basaltic composition with ages ranging from 81.4±0.69 Ma to 85.4±0.93 Ma (Santonian–Campanian), according to laser ablation inductively coupled mass spectrometry (LA-ICP-MS) dating of zircons in the rocks. These new U–Pb data, together with geothermobarometry calculations from the amphibolites and new geochemical interpretations, indicate that the metamorphic sole rocks formed on a subducted slab throughout the ophiolite generation in an SSZ environment.

Acknowledgements: I would like to thank Dr. Andrew Locock for performing mineral chemistry analyses and Dr. Laura Bracciali for LA-ICP-MS Zircon Analyses. The author is also indebted to the four anonymous reviewers and the Editor Milan Kohút for their constructive comments and suggestions, which greatly helped to improve the manuscript. Funding information: Financial supports from the Çukurova University Research Foundation (Project No: FBA-2018-10777).

References

Al-Riyami K., Robertson A., Dixon J. & Xenophontos C. 2002: Origin and emplacement of the Late Cretaceous Baer–Bassit ophiolite and its metamorphic sole in NW Syria. *Lithos* 65, 1, 225–260.

Anderson J.L. 1996: Status of thermobarometry in granitic batholiths. *Earth Environ. Sci. Trans. R Soc. Edinb.* 87, 125–138.

Anderson J.L., Barth A.P., Wooden J.L. & Mazdab F. 2008: Thermometers and thermobarometers in granitic systems. *Rev. Mineral. Geochem*. 69, 1, 121–142.

Armstrong J.T. 1988: Quantitative analysis of silicates and oxide minerals: Comparison of Monte-Carlo, ZAF and Phi-Rho-Z procedures. In: Newbury D.E. (Ed.): Microbeam Analysis. *San Francisco Press*, 239–246.

Bağcı U., Parlak O. & Höck V. 2005: Whole-Rock Mineral Chemistry of Cumulates from the Kızıldağ (Hatay) Ophiolite (Turkey): Clues for Multiple Magma Generation During Crustal Accretion in the Southern Neotethyan Ocean. *Mineral. Mag.* 69, 1, 53–76.

Bağcı U., Parlak O. & Höck V. 2008: Geochemistry and Tectonic Environment of Diverse Magma Generations Forming the Crustal Units of the Kızıldağ (Hatay) Ophiolite, southern Turkey. *Turk. J. Earth Scie.* 17, 43–71.

Bernard-Griffiths J., Peucat J.J., Sheppard S. & Vidal P. 1985: Petrogenesis of Hercynian leucogranites from the southern Armorican Massif: contribution of REE and isotopic (Sr, Nd, Pb and O) geochemical data to the study of source rock characteristics and ages. *Earth Planet. Sci. Lett.* 74, 2–3, 235–50.

Best M. G. 1982: Igneous and metamorphic petrology. *Freeman*, San Francisco, USA, 1–458.

Beyarslan M. & Bingöl A.F. 2000; Petrology of a suprasubduction zone ophiolite (Elazığ, Turkey). *Canad. J. Earth Sci.* 37, 1411–24.

Boudier F., Bouchez J.L., Nicolas A., Cannat M., Ceuleneer G., Misseri M. & Montigny R. 1985: Kinematics of oceanic thrusting in the Oman ophiolite: model of plate convergence. *Earth Planet. Sci. Lett.* 75, 215–222.

Boudier F., Ceuleneer G. & Nicolas A. 1988: Shear zones, thrusts and related magmatism in the Oman ophiolite: initiation of thrusting on an oceanic ridge. *Tectonophysics* 151, 275–296.

Brown E.H. 1977: The crossite content of ca-amphibole as a guide to pressure of metamorphism. *J. Petrol.* 18, 53–72. https://doi.org/10.1093/petrology/18.1.53

Calzolari G., Rossetti F., Ault A.K., Lucci F., Olivetti V. & Nozaem R. 2018: Hematite (U–Th)/He thermochronometry constrains intraplate strike-slip faulting on the Kuh-e Faghan Fault; central Iran. *Tectonophysics* 728, 41–54.

Çelik Ö.F. 2007: Metamorphic sole rocks and their mafic dykes in the eastern Tauride belt ophiolites (southern Turkey): İmplications for OIB type magma generation following slab break–off. *Geol. Mag.* 144, 849–866. https://doi.org/10.1017/S0016756807003573

Çelik Ö.F. 2008: Detailed geochemistry and K-Ar geochronology of the metamorphic sole rocks and their mafic dykes from the Mersin Ophiolite, Southern Turkey: *Turk. J. Earth Sci.* 17, 685–708.

Çelik Ö.F. & Delaloye M. 2003: Origin of metamorphic sole rocks and their postkinematic mafic dike swarms in the Antalya and Lycian ophiolites, SW Turkey. *Geol. J.* 38, 235–56.

Çelik Ö.F. & Delaloye M. 2006: Characteristics of ophioliterelated metamorphic rocks in the Beyşehir ophiolitic mélange (Central Taurides, Turkey), deduced from whole rock and mineral chemistry. *J. Asian Earth Sci.* 26, 461–476. https://doi.org/10.1016/j.jseaes.2004.10.008

Çelik Ö.F., Delaloye M. & Feraud G. 2004: $^{40}Ar/^{39}Ar$ dating and rapid cooling of the metamorphic sole rocks at the base of Tauride belt ophiolites, S Turkey. In: 5th Int. Symp. Eastern Mediterranean Geology, April 2004, Thessaloniki, Greece, 243–244.

Coleman R.G. 1981: Tectonic setting for ophiolite obduction in Oman. *J. Geophys. Res.* 86, 2497–2508.

Coombs D.S., Nakamura Y. & Vuangnat M. 1976: Pumpellyite–actinolite facies schists of the Taveyanne Formation near Loèche, Valais, Switzerland. *J. Petrol.* 17, 440–471.

Cruz-Uribe A.M., Feineman M.D., Zack T. & Barth M. 2014: Metamorphic reaction rates at ~650–800 °C from diffusion of niobium in rutile. *Geochim. Cosmochim. Acta* 130, 63–77.

Deer W.A., Howie R.A. & Zussman J. 1992: An introduction to the rock-forming minerals. *Prentice Hall*, 1–696.

Dewey J.F. 1976: Ophiolite obduction. *Tectonophysics* 31, 93–120.

Dewey J.F. & Casey J.F. 2013: The sole of an ophiolite: The Ordovician Bay of Islands Complex, Newfoundland. *J. Geol. Soc.* 170, 715–722.

Dilek Y. & Moores E.M. 1990: Regional tectonics of the eastern Mediterranean ophiolites. In: Malpas J., Moores E., Panayiotou A. & Xenophontos C. (Eds.): Ophiolites-oceanic crustal analogues. In: Proceedings of Troodos ophiolite symposium-1987, 295–309.

Dilek Y. & Thy P. 2006: Age and petrogenesis of plagiogranite intrusions in the Ankara mélange central Turkey. *Island Arc* 15, 44–57.

Dilek Y., Thy P., Hacker B. & Grundvig S. 1999: Structure and petrology of Tauride ophiolites and mafic dyke intrusions (Turkey): implications for the Neotethyan ocean. *Geol. Soc. Am. Bull.* 111, 1192–1216.

Donovan J.J., Snyder D.A & Rivers M.L. 1993: An Improved Interference Correction for Trace Element Analysis. *Microbeam Analysis* 2, 23–28.

Elmas A. & Yilmaz Y. 2003: Development of an oblique subduction zone – Tectonic evolution of the tethys suture zone in southeast Turkey. *International Geology Review* 45, 9, 827–840.

Ernst W.G. & Liu J. 1998: Experimental phase-equilibrium study of Al- and Ti-contents of calcic amphibole in MORB — A semiquantitative thermobarometer. *Am. Mineral.* 83, 952–969.

Ersoy Y.E. 2013: PETROMODELER (Petrological Modeler): a Microsoft® Excel© spreadsheet program for modelling melting, mixing, crystallization and assimilation processes in magmatic systems. *Turk. J. Earth Sci.* 22, 115–125.

Fergusson C.L. & Cawood P.A. 1994: Structural history of the metamorphic sole of the Bay of Islands Complex, western Newfoundland. *Can. J. Earth Sci.* 32, 533–544.

Floyd P. A., Kelling G. & Gökçen S. 1991: Geochemistry and tectonic environment of basaltic rocks from the Misis ophiolitic Mélange, South Turkey. *Chem. Geol.* 89, 263–280.

Floyd P.A., Göncüoğlu M.C., Winchester J.A. & Yalınız M.K. 2000: Geochemical character and tectonic environment of Neotethyan ophiolitic fragments and metabasites in the Central Anatolian crystalline complex, Turkey. In: Bozkurt E., Winchester J.A. & Piper J.D.A. (Eds.): Tectonics and magmatism in Turkey and the surrounding area. *Geol. Soc. London, Spec. Publ.* 173, 183–202.

Gartzos E., Dietrich V.J., Migiros G., Serelis K. & Lymperopoulou T.H. 2009: The origin of amphibolites from metamorphic soles beneath the ultramafic ophiolites in Evia and Lesvos (Greece) and their geotectonic implication. *Lithos* 108, 1, 4, 224–242.

Gnos E., & Peters T. 1993: K-Ar ages of the metamorphic sole of the Semail ophiolite: implications for cooling history. *Contrib. Mineral. Petrol.* 113, 325–332.

Görür N., Oktay F.Y., Seymen İ. & Şengör A.M.C. 1984: Paleotectonic evolution of Tuz Gölü basin complex, central Turkey. In: Dixon J.E. & Robertson A.H.F. (Eds.): The Geological Evolution of the Eastern Mediterranean. *Geol. Soc. London, Spec. Publ.* 17, 81–96.

Hacker B.R. 1990: Simulation of the Metamorphic and Deformational History of the Metamorphic Sole of the Oman Ophiolite. *J. Geophys. Res.* 95, 4895–4907.

Hacker B.R. 1991: The role of deformation in the formation of metamorphic gradients: Ridge subduction beneath the Oman Ophiolite. *Tectonics* 10, 455–473. https://doi.org/10.1029/ 90TC02779

Hacker B.R. 1994: Rapid emplacement of young oceanic lithosphere: Argon geochronology of the Oman ophiolite. *Science* 265, 1563–1565.

Hanson C.F. 1980: Rare earth elements in petrogenetic studies of igneous systems. *Ann. Rev. Earth Planet. Sci.* 8, 371–406.

Harms U., Cameron K.L., Simon K. & Bratz H. 1997: Geochemistry and petrogenesis of metabasites from the KTB ultradeep borehole, Germany. *Geol. Rundsch.* 86, 155–66.

Hawthorne F.C., Oberti R., Harlow G.E., Maresch W.V., Martin R.F., Schumacher J.C. & Welch M.D. 2012: IMA report, nomenclature of the amphibole supergroup. *Am. Mineral.* 97, 2031–2048.

Holland T. & Blundy J. 1994: Non-ideal interactions in calcic amphiboles and their bearing on amphibole-plagioclase thermometry. *Contrib. Miner. Petrol.* 116, 433–447

Jakes P. & Gill J. 1970: Rare earth elements and the island arc tholeiitic series. *Earth Planet. Sci. Lett.* 9, 17–28.

Jamieson R.A. 1980: Formation of metamorphic aureoles beneath ophiolites — Evidence from the St. Anthony Complex, Newfoundland. *Geology* 8, 3, 150–154.

John T., Klemd R., Klemme S., Pfänder J.A., Hoffmann J.E. & Gao J. 2011: Nb–Ta fractionation by partial melting at the titanite-rutile transition. *Contrib. Mineral. Petrol.* 161, 35–45.

Johnson M.C. & Rutherford M.J. 1989: Experimental calibration of the aluminum in hornblende geobarometer with application to long valley caldera (California) Volcanic Rocks. *Geology* 17, 837–841.

Kakar M.I. & Khalid M. 2015: Petrology and geochemistry of amphibolites and greenschists from the metamorphic sole of the Muslim Bagh ophiolite (Pakistan): implications for protolith and ophiolite emplacement. *Arab. J. Geosci.* 8, 6105–6120.

Karaoğlan F. 2012: Geochronology of the Ophiolitic and Granitic Rocks along the SE Anatolian Orogen. *PhD Thesis. Çukurova University*, Adana, 1–288 (in Turkish with English abstract).

Ketin İ. 1983: A general view of the geology of Turkey. *Istanbul Teknik Üniversitesi Matbaası*, Istanbul, 1–596 (in Turkish).

Krenn K., Kaindl R. & Hinkes G. 2004: Pumpellyite in metapelites of the Schneeberg Complex (eastern Alps, Austria): a relict of the eo-Alpine prograde P–T path? *Eur. J. Mineral.* 16, 661–669.

Kroner A., Williams I.S., Compston W., Baur N., Vitanage P.W. & Perera L.R.L. 1987: Zircon ion microprobe dating of high-grade rocks in Sri Lanka. *J. Geol.* 95, 775–791.

Lanphere M.A., Coleman R.G., Karamata S. & Pamić J. 1975: Age of amphibolites associated with Alpine peridotites in the Dinaride ophiolite zone, Yugoslavia. *Earth Planet. Sci. Lett.* 26, 271–276.

Leake B.E. & Woolley Arps C.E.S. 1997: Nomenclature of amphiboles: report of the Subcommittee on Amphiboles of the International Mineralogical Association, Commission on New Minerals and Mineral Names. *Am. Mineral.* 82, 1019–1037.

Liou J.G. & Ernst W.G. 1979: Oceanic ridge metamorphism of the East Taiwan Ophiolite. *Contrib. Mineral. Petrol.* 68, 335–342.

Locock A.J. 2014: An Excel spreadsheet to classify chemical analyses of amphiboles following the IMA 2012 recommendations. *Comput. Geosci.* 62, 1–11

Lucassen F., Dulski P., Abart R., Franz G., Rhede D. & Romer R.L. 2010: Redistribution of HFSE elements during rutile replacement by titanite. *Contrib. Mineral. Petrol.* 160, 279–295.

Lucci F., Della Ventura G., Conte A., Nazzari M. & Scarlato P. 2018: Naturally Occurring Asbestos (NOA) in Granitoid Rocks: A Case Study from Sardinia (Italy). *Minerals* 8, 10, 442.

Ludwig K.R. 2003: User's Manual for Isoplot 3.00: A Geochronological Toolkit for Microsoft Excel. *Special Publication/Berkeley Geochronology Center* 74.

Luvizotto G.L. & Zack T. 2009: Nb and Zr behavior in rutile during high-grade metamorphism and retrogression: an example from the Ivrea Verbano Zone. *Chem. Geol.* 261, 303–317.

Luvizotto G.L., Zack T., Triebold S., & von Eynatten H. 2009: Rutile occurrence and trace element behavior in medium-grade metasedimentary rocks: example from the Erzgebirge, Germany. *Mineral. Petrol.* 97, 233–249.

Lytwyn J.N & Casey J.F. 1995: The geochemistry of postkinematic mafic dyke swarms and subophiolitic metabasites, Pozanti–Karsanti ophiolite, Turkey: Evidence for ridge subduction. *Geol. Soc. Am. Bull.* 107, 830–850.

Malpas J. 1979: The dynamothermal aureole of the Bay of Islands ophiolite suite. *Can. J. Earth Sci.* 16, 2086–2101. https://doi.org/10.1139/e79-198

Meinhold G. 2010: Rutile and its applications in earth sciences. *Earth Sci. Rev.* 102, 1–28.

Mullen E.D. 1983: $MnO/TiO_2/P_2O_5$: a minor element discriminant for basaltic rocks of oceanic environnement and its implication for petrogenesis. *Earth Planet. Sci. Lett.* 62, 53–62.

Nishimura Y., Coombs D.S., Landis C.A. & Itaya T. 2000: Continuous metamorphic gradient documented by graphitization and K–Ar age, southeast Otago, New Zealand. *Am. Mineral.* 85, 1625–1636.

Nurlu N. 2009: Origin of the İspendere (Malatya) ophiolite. *MSc Thesis, Çukurova Üniversitesi, Fen Bilimleri Enstitüsü*, Adana, Turkey.

Nurlu N. 2016: Geochemistry and Tectonic Signifiance of the Tectonomagmatic Units in the Helete (Kahramanmaraş) Region. *PhD Thesis, Çukurova University Intitute of Natural and Applied Sciences*, 1–281.

Nurlu N., Parlak O., Robertson A.H.F. & Quadt A. 2016: Implications of Late Cretaceous U–Pb zircon ages of granitic intrusions cutting ophiolitic and volcanogenic rocks for the assembly of the Tauride allochton in SE Anatolia (Helete area, Kahramanmaraş Region, SE Turkey). *Int. J. Earth Sci.* 105, 283–314.

Okay A.I. & Tüysüz O. 1999: Tethyan sutures of northern Turkey. In: Durand B., Jolivet F. & Séranne M. (Eds.): The Mediterranean Basins: Tertiary extension within the Alpine orogeny. *Geol. Soc. London, Spec. Publ.* 516, 475–515.

Önen A.P. & Hall R. 1993: Ophiolites and related metamorphic rocks from the Kütahya region, NE Turkey. *Geol. J.* 28, 399–412.

Özek G., Akgül M., Nurlu N. & Yapıcı N. 2017: Tectonic Setting and Geochemical Features of the Guleman Ophiolite (Elazığ). *KSU Journal of Engineering Sciences* 20, 2, 29–44.

Parlak O. 1996: Geochemistry and geochronology of the Mersin ophiolite within the eastern Mediterranean tectonic frame. *PhD Thesis, Terre Environ.* 6, Univ. Geneva, 1–242.

Parlak O. 2000: Geochemistry and significance of mafic dyke swarms in the Pozantı-Karsantı ophiolite (southern Turkey). *Turkish J. Earth Sci.* 24, 29–38.

Parlak O. 2006: Geodynamic significance of granitoid magmatism in the southeast Anatolian orogen: geochemical and geochronological evidence from Göksun–Afşin (Kahramanmaraş, Turkey) region. *Int. J. Earth Sci. (Geol. Rundsch.)* 95, 609–627

Parlak O. 2016: The Tauride Ophiolites of Anatolia (Turkey): A Review. *J. Earth Sci.* 27, 901–934.

Parlak O. & Delaloye M. 1996: Geochemistry and timing of postmetamorphic dike emplacement in the Mersin ophiolite (southern Turkey): new age constraints from 40Ar/39Ar geochronology. *Terra Nova* 8, 585–592.

Parlak O. & Delaloye M. 1999: Precise $^{40}Ar/^{39}Ar$ ages from the metamorphic sole of the Mersin ophiolite (southern Turkey). *Tectonophysics* 301, 145–158.

Parlak O. & Robertson A.H.F. 2004: The Ophiolite-Related Mersin Mélange, Southern Turkey: Its Role in the Tectonic- Sedimentary Setting of Tethys in the Eastern Mediterranean Region. *Geol. Mag.* 141, 3, 257–286.

Parlak O., Delaloye M. & Bingöl E. 1995: Geochemistry of the volcanic rocks in the Mersin ophiolite (Southern Turkey) and their tectonic significance in the eastern Mediterranean geology. In: Pişkin Ö., Ergün M., Savaşçın M.Y. & Tarcan G. (Eds.): International Earth Science Colloquium on the Aegean Region. *IESCA 1995*, 4, 41–63.

Parlak O., Höck V. & Delaloye M. 2000: Suprasubduction zone origin of the Pozantı– Karsanti ophiolite (southern Turkey) deduced from whole-rock and mineral chemistry of the gabbroic cumulates. In: Bozkurt E., Winchester J.A. & Piper J.D.A. (Eds.): Tectonics and Magmatism in Turkey and the Surrounding Area. *Geol. Soc. London, Spec. Publ.* 173, 219–234.

Parlak O., Höck V., Kozlu H. & Delaloye M. 2004: Oceanic crust generation in an island arc tectonic setting, SE Anatolian Orogenic Belt (Turkey). *Geol. Mag.* 141, 583–603.

Parlak O., Yılmaz H., Boztuğ D. & Höck V. 2005: Geochemistry and tectonic setting of the Divriği ophiolite in the east central Anatolia (Sivas, Turkey): evidence for melt generation within an asthenospheric window prior to ophiolite emplacement onto the Taurides. In: International Symposium on the Geodynamics of Eastern Mediterranean: Active Tectonics of the Aegean Region, 15-18 June 2005, *Kadir Has University*, İstanbul, Turkey, 1– 224.

Parlak O., Rizaoğlu T., Bağci U., Karaoğlan F. & Höck V. 2009: Tectonic significance of the geochemistry and petrology of ophiolites in southeast Anatolia, Turkey. *Tectonophysics* 473, 173–187.

Passaglia E. & Gottardi G. 1973: Crystal chemistry and nomenclature of pumpellyites and julgoldites. *Can. Mineral.* 12, 219–233.

Pearce J.A. 1982: Trace element characteristics of lavaş from destructive plate boundries. In: R.S. Thorpe (Ed.): Andesites. *Wiley*, New York, 525–48.

Pearce J.A. 1983: Role of the sub-continental lithosphere in magma genesis at active continental margins. In: Hawkesworth C.J. & Norry M.J. (Eds.): Continental Basalts and Mantle Xenoliths. *Shiva*, Nantwich, 230–249.

Pearce J.A. & Cann J.R. 1973: Tectonic setting of basaltic volcanic rocks determined using trace element analysis. *Earth Planet. Sci. Lett.* 19, 290–300.

Pearce J.A. & Norry M.J. 1979: Petrogenetic implications of Ti, Zr, Y and Nb variations in volcanic rocks. *Contrib. Mineral. Petrol.* 69, 33–47.

Pearce J. A., Lippard S. J. & Roberts S. 1984: Characteristics and tectonic significance of suprasubduction zone ophiolites. In: Kokelaar B.P. & Hewells M.F. (Eds.): Marginal Basin Geology. *Geol. Soc. London, Spec. Publ.* 16, 77–94.

Perinçek D. 1979: The Geology of Hazro-Korudağ-Çüngüş-Maden-Ergani-Hazar-Elazığ-Malatya Area: Guide book. *Türkiye Jeoloji Kurumu Yayını* , 1–33.

Perinçek D. & ve Fren A.G. 1990: Origin of the Amik Basin, Developing in the Domain of Eastern Anatolia and Dead Sea Fault Zones with Directional Pulse: Türkiye 8. *Petrol Kongresi Bildirileri*, Ankara.

Poisson A. 1986: The Anatolian micro-continent in the Journal of Geology eastern Mediterranean context. the Neo-Tethian troughs. *Sci. Terre Mem*. 47, 311–328.

Potel S., Schmidt S.T. & De Capitani C. 2002: Composition of pumpellyite, epidote and chlorite from New Caledonia. How important are metamorphic grade and whole-rock composition? *Schweiz. Mineral. Petrogr. Mitt.* 82, 229–252.

Rizaoğlu T., Parlak O., Höck V. & İşler F. 2006: Nature and significance of Late Cretaceous ophiolitic rocks and its relation to the Baskil granitoid in Elazığ region, SE Turkey. *Geol. Soc. London, Spec. Publ.* 260, 327–350.

Roberts N.M.W., Thomas R. & Jacobs J. 2016: Geochronological constraints on th metamorphic sole of the Semail ophiolite in the United Arab Emirates. *Geoscience Frontiers* 7, 609–619.

Robertson A.H.F. 2002: Overview of the genesis and emplacement of Mesozoic ophiolites in the eastern Mediterranean Tethyan region. *Lithos* 65, 1–67.

Robertson A.H.F. 2004: Development of concepts concerning the genesis and emplacement of Tethyan ophiolites in the eastern Mediterranean and Oman regions. *Earth-Sci. Rev.* 66, 331–387.

Robertson A.H.F. & Dixon J.E. 1984: Introduction: aspects of the geological evolution of the Eastern Mediterranean. In: Dixon J.E. & Robertson A.H.F. (Eds.): The Geological Evolution of the Eastern Mediterranean. *Geol. Soc. London, Spec. Publ.* 17, 1–74.

Robertson A.H.F., Ustaömer T., Parlak O., Ünlügenç U., Taşli K. & İnan N. 2006: The Berit transect of the Tauride thrust belt, S Turkey: Late Cretaceous–Early Cenozoic accretionary/collisional processes related to closure of the Southern Neotethys. *J. Asian Earth Sci.* 27, 108–145.

Robertson A.H. F., Parlak O., Rizaoğlu T., Ünlügenç Ü., İnan N., Tasli K. & Ustaömer T. 2007: Tectonic evolution of the South Tethyan ocean: evidence from the Eastern Taurus Mountains (Elazığ region, SE Turkey). *Geol. Soc. London, Spec. Publ.* 272, 231–270.

Rossetti F., Monié P., Nasrabady M., Theye T., Lucci F. & Saadat M. 2017: Early Carboniferous subduction-zone metamorphism preserved within the Palaeo-Tethyan Rasht ophiolites (western Alborz, Iran). *J. Geol. Soc.* 130, 1–18.

Rudnick R.L. & Fountain D.M. 1995: Nature and composition of the continental crust: A lower crustal perspective. *Rev. Geophys*. 33. https://doi.org/10.1029/95RG01302

Rudnick R.L. & Gao S. 2003: The composition of the continental crust. In: Rudnick R.L., Holland H.D. & Turekian K.K. (Eds.): Treatise on Geochemistry – The Crust. *Elsevier*, Oxford, 1–64.

Searle M.P. & Cox J. 2002: Subduction zone metamorphism during formation and emplacement of the Semail ophiolite in the Oman Mountains. *Geol. Mag.* 139, 3, 241–255.

Searle M.P. & Malpas J. 1980: The structure and metamorphism of rocks beneath the Semail ophiolite of Oman and their significance in ophiolite obduction. *Trans. R. Soc. Edinb. Earth Sci.* 71, 247–262.

Shervais J.W. 1982: Ti–V plots and the petrogenesis of modern and ophiolitic lavas. *Earth Planet. Sci. Lett.* 59, 1, 101–118.

Shimzu N. & Arculus R.J. 1975: Rare earth concentrations in a suite of basanitoids and alkali olivine basalts from Grenada, Lesser Antilles. *Contrib. Mineral. Petrol.* 50, 231–240.

Spray J.G. 1984: Possible causes and consequences of upper mantle decoupling and ophiolite displacement. In: Gass I.G., Lippard S.J. & Shelton A.W. (Eds.): Ophiolites and oceanic lithosphere. *Geol. Soc. London, Spec. Publ.* 13, 255–268.

Spray J.G., & Roddick J.C. 1980: Petrology and 40Ar/39Ar geochronology of some Hellenic sub-ophiolite metamorphic rocks. *Contrib. Mineral. Petrol.* 72, 43–55.

Spray J. G., Bebien J., Rex D. C. & Roddick J. C. 1984: Age constraints on the igneous and metamorphic evolution of the Hellenic-Dinaric ophiolites. *Geol. Soc. London, Spec. Publ.* 17, 619–627.

Sun S. S. & McDonough W. F. 1989: Chemical and isotopic systematics of oceanic basalts: Implications for mantle composition and processes. In: Saunders A.D. & Norry M.J. (Eds.): Magmatism in the Ocean Basins. *Geol. Soc. London, Spec. Publ.* 42, 3, 13–45.

Şengör A.M.C. & Yılmaz Y. 1981: Tethyan evolution of Turkey: A plate tectonic approach. *Tectonophysics* 75, 181–241. https://doi.org/10.1016/0040-1951(81)90275-4

Teipel U., Eichhorn R., Loth G., Rohrmüller J., Höll R. & Kennedy A. 2004: U–Pb SHRIMP and Nd isotopic data from the western bohemian massif (Bayerischer Wald, Germany): implications for upper Vendian and lower Ordovician magmatism. *Int. J. Earth Sci.* 93, 782–801.

Vavra G., Gebauer D., Schmid R. & Compston W. 1996: Multiple zircon growth and recrystallization during polyphaseLate Carboniferous to Triassic metamorphism in granulitesof the Ivrea Zone (Southern Alps): an ion microprobe (SHRIMP) study. *Contrib. Mineral. Petrol.*122, 337–358.

Vavra G., Schmid R. & Gebauer D. 1999: Internal morphology, habit and U–Th–Pb microanalysis of amphibolite-to-granulite facies zircons: geochronology of the Ivrea Zone (Southern Alps). *Contrib. Mineral. Petrol.* 134, 380–404.

Vergili Ö. & Parlak O. 2005: Geochemistry and tectonic setting of metamorphic sole rocks and mafic dikes from the P›narbafl› (Kayseri) ophiolite, central Anatolia. *Ofioliti* 30, 37–52.

Wakabayashi J., Ghatak A. & Basu A.R. 2010: Supra-subduction-zone ophiolite generation, emplacement, and initiation of subduction: A perspective from geochemistry, metamorphism, geochronology, and regional geology. *Geol. Soc. Am. Bull.* 122, 1548–1568. https://doi.org/10.1130/B30017.1

Williams H. & Smyth W.R. 1973: Metamorphic aureoles beneath ophiolite suites and Alpine peridotites: Tectonic implications with west Newfoundland examples. *Am. J. Sci*. 273, 594–621.

Winchester J. A. & Floyd P. A. 1977: Geochemical discrimination of different magma series and their differentiation products using immobile elements. *Chem. Geol.* 16, 325–43.

Watson E.B. 1996: Dissolution, growth and survival of zircons during crustal fusion: Kinetic principles, geological models and implications for isotopic inheritance. *Trans. Royal Soc. Edinburgh: Earth Sci.* 87, 43–56.

Yaliniz K.M., Floyd P. & Göncüoğlu M.C. 1996: Suprasubduction zone ophiolites of Central Anatolia: geochemical evidence from the Sarıkaraman ophiolite, Aksaray, Turkey. *Mineral. Mag.* 60, 697–710.

Yaliniz K.M., Floyd P. & Göncüoğlu M.C. 2000: Geochemistry of volcanic rocks from the Çiçekdağ ophiolite, central Anatolia, Turkey, and their inferred tectonic setting within the northern branch of the Neotethyan ocean. In: Bozkurt E., Winchester J.A. & Piper J.D.A (Eds.): Tectonics and Magmatism in Turkey and the Surrounding area. *Geol. Soc. London, Spec. Publ.* 173, 203–218.

Yang T.N. 2004: Retrograded textures and associated mass transfer: evidenc for aqueous fluid action during exhumation of the Qinglongshan eclogite Southern Sulu ultrahigh pressure metamorphic terrane, eastern China. *J. Metamorph. Geol.* 22, 653–669.

Yazgan E. & Chessex R. 1991: Geology and Tectonic Evolution of the Southeastern Taurides in the Region of Malatya. *Turk. Assoc. Petrol. Geol.* 3, 1–42.

Yiğitbaş E. & Yilmaz Y. 1996: New evidence and solution to Maden Complex controversy of the southeast Anatolian orogen (Turkey). *Geol. Rundsch*. 85, 250–263.

Yiğitbaş E., Yilmaz Y. & Genç Ş.C. 1992: Eocene thrust settlement in the Southeastern Anatolia Orogenic Belt. In: Tür. 9. Petrol. Kong. Tebliğler, 307–318 (in Turkish).

Yılmaz Y. 1984: Geology of the Amanos mountains. In: Türkiye Petrolleri Anonim Ortaklığı Rapor., 1–4.

Yilmaz Y. 1993: New evidence and model on the evolution of the southeast Anatolian orogen. *Geol. Soc. Am. Bull.* 105, 251–271.

Yilmaz Y., Yiğitbaş E. & Genç Ş.C. 1993: Ophiolitic and Metamorphic Assemblages of Southeast Anatolia and their Significance in the Geological Evolution of the Orogenic Belt. *Tectonics* 12, 1280–1297.

Zack T., Kronz A., Foley S.F. & Rivers T. 2002: Trace element abundances in rutiles from eclogites and associated garnet mica schists. *Chem. Geol.* 184, 97–122.

Supplement

Table S1: LA–ICP–MS method.

U–(Th)–Pb dating method, CAF, Stellenbosch University, South Africa – Metadata table.
U–(Th)–Pb Geochronology Method.

Laser ablation U–Pb data were collected at the Central Analytical Facilities, Stellenbosch University, using a 193 nm wavelength ASI Resolution laser ablation system coupled to a Thermo Scientific Element 2 single collector magnetic sector field inductively coupled plasma mass spectrometer (SC–SF–ICP–MS). U–Pb data and metadata are tabulated in Supplementary material.
At the start of each analytical session the mass spectrometer was tuned by ablating a line scan on the NIST620 glass. The torch position, lenses and gas flows were tuned while measuring ^{206}Pb, ^{238}U and $^{238}U^{16}O$ to get stable signals and high intensity on ^{206}Pb and ^{238}U, as well as low oxide rates ($^{238}U^{16}O/^{238}U$ <0.3 %). The ablated zircon material was transported from the laser cell into the ICP–MS using a continuous flow of 0.35 l/min of He gas. Signals of m/z ^{202}Pb, ^{204}Pb, ^{206}Pb, ^{207}Pb, ^{208}Pb, ^{232}Th, ^{235}U and ^{238}U were acquired in electrostatic scan mode. The ^{202}Hg signal was collected in order to correct the isobaric interference of ^{204}Hg on ^{204}Pb. The laser and ICP–MS software packages were synchronized in order to allow automated execution of the analysis. One analytical session can include up to 500 measurements.
The laser sampling protocol employed a 26 µm static spot and a fluence of 2.0 J/cm^2. Before the gas blank measurement, each spot was pre-ablated by firing two laser shots to remove common Pb from the surface that may have been introduced during the sample preparation.
During each analytical session the zircon reference materials GJ-1 (Jackson et al. 2004) and Plešovice (Sláma et al. 2008) were measured between groups of 13 unknowns. Zircon GJ-1 was used as a matrix-matched primary reference material to correct for mass discrimination on measured isotope ratios in unknown samples and simultaneous correction for instrumental drift. The values used for normalization are based on ratios determined by ID-TIMS reported in Horstwood et al. (2016). Plešovice zircon was used as secondary reference material to validate the results and assess the quality of the data for each analytical session.
Data reduction was performed with the software package Iolite v.3.5 (Paton et al. 2011), combined with Vizual Age (Petrus & Kamber 2012). An exponential model of laser-induced elemental fractionation (LIEF) obtained by combining the isotopic ratios of the primary reference material from the entire session is used to correct for time-dependent down-hole elemental fractionation in the unknowns, under the assumption of same fractionation behaviour in the reference material and the unknowns. After correction for LIEF and drift and normalization to the main reference material (performed in Iolite), uncertainty components for systematic errors are propagated by quadratic addition following the recommendations of Horstwood et al. (2016).

Laboratory & Sample Preparation	
Laboratory name	Central Analytical Facilities, Stellenbosch University, South Africa
Sample type/mineral	Igneous and metamorphic zircons
Sample preparation	Conventional mineral separation, 1 inch resin mount, 1 µm polish to finish
Imaging	CL, ZEISS Merlin SEM, 11 nA, 10 kV, 10 mm working distance
Laser ablation system	
Make, Model & type	ASI Resolution M-50-LR Excimer laser
Ablation cell & volume	Laurin Technic M-50 dual-volume cell
Laser wavelength	193 nm
Pulse width	15 ns
Fluence	2.0 J/cm^{-2}
Repetition rate	7 Hz
Spot size	26 µm
Sampling mode/pattern	Static spot ablation
Carrier gas	100 % He in the cell, Ar make-up gas combined using a T-connector close to sample cell
Pre-ablation background collection	13 s
Ablation duration	29 s
Wash-out delay	20 s
Cell carrier gas flow	0.35 l/min He
ICP-MS Instrument	
Make, Model & type	Thermo Scientific Element2 single collector HR-SF-ICP-MS
Sample introduction	via conventional tubing
RF power	1325 W
Make-up gas flow	0.9 l/min Ar
Detection system	Single collector secondary electron multiplier
Masses measured	202, 204, 206, 207, 208, 232, 235, 238
Integration time per peak (segment duration)	7, 14, 15, 18, 8, 8, 1, 13 ms, respectively
Total integration time per output datapoint	0.1 s
Sensitivity	0.3 % U
Dead time	6 ns
Data Processing	
Gas blank	13 s
Calibration strategy	GJ-1 used as primary reference material, Plešovice used as secondary reference material
Reference Material info	GJ-1 (Jackson et al. 2004); Plešovice (Slama et al. 2008)
Data processing package used/ Correction for LIEF	Iolite data reduction software package; LIEF modelled within each analytical session on the basis of combined analyses of the main reference material. LIEF correction assumes reference material and samples behave identically.
Mass discrimination	Reference material-sample bracketing with $^{207}Pb/^{206}Pb$ and $^{206}Pb/^{238}U$ normalized to zircon GJ-1
Common-Pb correction	No common Pb correction applied to the data
Uncertainty level & propagation	Decay constant uncertainties, ratio uncertainty of primary reference material and long-term excess variance of secondary reference material propagated by quadratic addition. Age uncertainties quoted at the 2s absolute level.
Quality control/Validation	Plešovice: Wtd avg $^{206}Pb/^{238}U$ age=336.2±0.8 Ma (2s, MSWD=1.1; n=30)

References

Horstwood M.S.A., Košler J., Gehrels G., Jackson S.E., McLean N.M., Paton C., Pearson N.J., Sircombe K., Sylvester P., Vermeesch P., Bowring J.F., Condon D.J. & Schoene B. 2016: Community-Derived Standards for LA–ICP–MS U–(Th–)Pb Geochronology – Uncertainty Propagation, Age Interpretation and Data Reporting. *Geostandards and Geoanalytical Research* 40, 3, 301–332.
Jackson S.E., Pearson N.J., Griffin W.L. & Belousova E.A. 2004: The application of laser ablation-inductively coupled plasma-mass spectrometry to in situ U–Pb zircon geochronology. *Chem. Geol.* 211, 47–69.
Paton C., Hellstrom J., Paul B., Woodhead J., Hergt J. 2011: Iolite: freeware for the visualisation and processing of mass spectrometric data: *J. Anal. At. Spectrom.* 26, 2508–2518.
Petrus J.A. & Kamber, B.S. 2012: VizualAge: A Novel Approach to Laser Ablation ICP-MS U-Pb Geochronology Data Reduction. *Geostandards and Geoanalytical Research* 36, 247–270.
Sláma J., Košler J., Condon D.J., Crowley J.L., Gerdes A., Hanchar J.M., Horstwood M.S.A., Morris G.A., Nasdala L., Norberg N.,Schaltegger U., Schoene B., Tubrett M.N. & Whitehouse M.J. 2008: Plešovice zircon – a new natural reference material for U-Pb and Hf isotopic microanalysis. *Chem. Geol.* 241, 1–35.

Table S2: Laser ablation SC–SF–ICP–MS U–Pb zircon data.

Identifier	206Pb (CPS)	204Pb (CPS)	206Pb/204Pb	U (mg/g)	Th/U	Data for Tera-Wasserburg plot				Data for Wetherill plot					Dates (Ma)									Concordance (%)
						238U/206Pb	2 s	$^{207}Pb/^{206}Pb$	2 s	$^{207}Pb/^{235}U$	2 s	$^{206}Pb/^{238}U$	2 s	rho	$^{207}Pb/^{206}Pb$	2 s	$2s_{sys}$		$^{206}Pb/^{238}U$	2 s	$2s_{sys}$	$^{207}Pb/^{235}U$	2 s	$2s_{sys}$	206/238 - 207/235
MG1 - 1	6.8.E+03	b.d.	b.d	104	0.36	80.13	1.99	0.0650	0.0049	0.1150	0.0097	0.0125	0.0003	0.29	600	150	159	1	79.9	2.0	2.5	109	9	11	73
MG1 - 2	4.0.E+03	b.d.	b.d	60	0.25	77.52	2.28	0.0639	0.0063	0.1090	0.0100	0.0129	0.0004	0.32	430	190	209	2	82.6	2.4	2.9	105	10	10	79
MG1 - 4	7.4.E+03	b.d.	b.d	106	0.28	79.68	1.65	0.0530	0.0035	0.0924	0.0062	0.0126	0.0003	0.31	190	130	150	3	80.4	1.7	2.2	89	6	7	91
MG1 - 5	1.3.E+04	b.d.	b.d	197	0.41	80.52	1.62	0.0499	0.0029	0.0847	0.0048	0.0124	0.0003	0.36	120	110	136	4	79.6	1.6	2.1	83	5	4	96
MG1 - 6	5.6.E+03	b.d.	b.d	87	0.29	78.19	2.26	0.0590	0.0059	0.1003	0.0096	0.0128	0.0004	0.30	320	190	218	5	81.9	2.4	2.8	96	9	10	85
MG1 - 7	2.6.E+03	b.d.	b.d	40	0.25	79.74	2.73	0.0650	0.0070	0.1090	0.0110	0.0125	0.0004	0.34	430	220	227	6	80.3	2.8	3.1	103	10	12	78
MG1 - 8	8.9.E+03	b.d.	b.d	135	0.30	77.58	1.75	0.0597	0.0037	0.1065	0.0067	0.0129	0.0003	0.36	480	130	135	7	82.6	1.9	2.3	103	6	7	81
MG1 - 9	8.9.E+03	b.d.	b.d	136	0.31	77.16	1.85	0.0546	0.0039	0.0959	0.0067	0.0130	0.0003	0.34	250	140	161	8	83.0	1.9	2.5	93	6	7	90
MG1 - 10	4.0.E+03	b.d.	b.d	59	0.23	76.75	1.94	0.0585	0.0048	0.1037	0.0084	0.0130	0.0003	0.31	300	160	180	9	83.5	2.1	2.5	99	8	9	85
MG1 - 11	4.4.E+03	b.d.	b.d	66	0.30	78.68	2.04	0.0662	0.0059	0.1136	0.0094	0.0127	0.0003	0.31	530	180	187	10	81.4	2.1	2.6	108	9	10	76
MG1 - 12	3.4.E+03	b.d.	b.d	47	0.23	71.79	2.47	0.1040	0.0100	0.2030	0.0210	0.0139	0.0005	0.33	1320	210	214	11	89.1	3.0	3.5	184	18	22	48
MG1 - 13	5.5.E+03	b.d.	b.d	81	0.26	76.28	1.80	0.0616	0.0048	0.1093	0.0080	0.0131	0.0003	0.32	430	150	167	12	83.9	2.0	2.5	104	7	9	81
MG1 - 14	6.1.E+03	b.d.	b.d	89	0.28	75.13	1.75	0.0537	0.0045	0.0971	0.0079	0.0133	0.0003	0.29	160	150	189	13	85.2	1.9	2.5	93	7	9	92
MG1 - 15	1.9.E+04	b.d.	b.d	270	0.91	81.23	1.72	0.0499	0.0028	0.0850	0.0047	0.0123	0.0003	0.38	150	120	131	14	78.9	1.7	2.1	83	4	5	96
MG1 - 16	1.0.E+04	b.d.	b.d	134	0.31	71.84	1.55	0.1224	0.0074	0.2340	0.0140	0.0139	0.0003	0.36	1810	120	121	15	89.1	1.9	2.5	210	12	15	42
MG1 - 17	1.2.E+04	b.d.	b.d	174	0.36	71.23	1.72	0.0529	0.0038	0.1018	0.0073	0.0140	0.0003	0.34	260	150	164	16	89.9	2.2	2.7	98	7	7	92
MG1 - 18	8.1.E+03	b.d.	b.d	122	0.39	76.51	1.81	0.0599	0.0045	0.1072	0.0080	0.0131	0.0003	0.32	410	150	163	17	83.7	2.0	2.5	103	7	8	82
MG1 - 19	1.2.E+04	b.d.	b.d	189	0.50	75.70	1.89	0.0513	0.0038	0.0922	0.0069	0.0132	0.0003	0.33	140	140	171	18	84.6	2.1	2.6	89	6	7	95
MG1 - 20	6.1.E+03	b.d.	b.d	91	0.32	78.13	1.77	0.0509	0.0037	0.0898	0.0066	0.0128	0.0003	0.31	110	130	168	19	82.0	1.9	2.4	87	6	7	95
MG1 - 21	5.0.E+03	b.d.	b.d	71	0.22	77.16	1.79	0.0525	0.0043	0.0947	0.0077	0.0130	0.0003	0.28	120	150	187	20	83.0	1.9	2.4	91	7	9	92
MG1 - 22	8.0.E+03	b.d.	b.d	115	0.34	76.75	1.47	0.0487	0.0030	0.0877	0.0053	0.0130	0.0003	0.32	70	120	145	21	83.4	1.6	2.2	85	5	5	98
MG1 - 23	7.0.E+03	b.d.	b.d	106	0.32	76.22	1.92	0.0675	0.0055	0.1168	0.0091	0.0131	0.0003	0.32	610	160	170	22	84.0	2.1	2.6	112	8	9	75
MG1 - 24	3.5.E+04	b.d.	b.d	550	0.65	80.52	1.56	0.0549	0.0021	0.0939	0.0037	0.0124	0.0002	0.49	350	79	86	23	79.6	1.5	2.1	91	4	4	88
MG1 - 25	2.4.E+04	b.d.	b.d	385	0.46	78.74	2.17	0.0469	0.0030	0.0819	0.0055	0.0127	0.0004	0.41	40	130	153	24	81.3	2.2	2.7	80	5	6	102
MG1 - 26	8.4.E+03	b.d.	b.d	120	0.44	74.18	1.71	0.0535	0.0034	0.0978	0.0061	0.0135	0.0003	0.37	220	130	144	25	86.3	1.9	2.5	94	6	7	92
MG1 - 27	7.7.E+03	b.d.	b.d	119	0.35	79.11	1.82	0.0545	0.0034	0.0950	0.0060	0.0126	0.0003	0.36	290	130	140	26	81.0	1.8	2.3	91	6	7	89
MG1 - 28	9.5.E+03	b.d.	b.d	141	0.49	79.87	1.66	0.0513	0.0033	0.0873	0.0053	0.0125	0.0003	0.34	140	120	148	27	80.2	1.6	2.2	84	5	6	95
MG1 - 29	5.0.E+03	b.d.	b.d	72	0.37	74.35	1.99	0.0816	0.0059	0.1480	0.0100	0.0135	0.0004	0.40	960	150	152	28	86.1	2.3	2.8	139	9	10	62
MG1 - 30	6.2.E+03	b.d.	b.d	93	0.31	78.13	1.71	0.0549	0.0038	0.0962	0.0066	0.0128	0.0003	0.32	210	130	155	29	81.9	1.8	2.4	92	6	7	89
MG1 - 31	8.4.E+03	b.d.	b.d	126	0.33	78.68	1.67	0.0501	0.0034	0.0866	0.0058	0.0127	0.0003	0.32	110	130	158	30	81.4	1.7	2.3	84	6	6	97
MG2 - 2	7.3.E+04	b.d.	b.d	1068	0.15	74.02	1.21	0.0490	0.0012	0.0905	0.0024	0.0135	0.0002	0.61	137	52	59	1	86.5	1.4	2.1	88	2	3	98
MG2 - 3	1.1.E+05	b.d.	b.d	1526	0.71	73.53	1.14	0.0494	0.0010	0.0919	0.0022	0.0136	0.0002	0.65	156	46	49	2	87.1	1.3	2.1	89	2	3	98
MG2 - 4	1.1.E+05	b.d.	b.d	1466	0.20	75.13	1.13	0.0489	0.0014	0.0898	0.0027	0.0133	0.0002	0.50	131	61	68	3	85.2	1.3	2.0	87	3	3	98
MG2 - 5	1.3.E+05	b.d.	b.d	1805	0.40	69.88	0.98	0.0484	0.0008	0.0955	0.0020	0.0143	0.0002	0.67	115	36	40	4	91.6	1.3	2.1	93	2	3	99
MG2 - 6	1.9.E+05	b.d.	b.d	3135	0.09	76.39	1.81	0.0515	0.0016	0.0923	0.0032	0.0131	0.0003	0.68	240	68	72	5	83.8	2.0	2.5	90	3	3	94
MG2 - 7	2.6.E+05	b.d.	b.d	3930	0.95	74.63	1.06	0.0496	0.0007	0.0911	0.0018	0.0134	0.0002	0.72	171	33	36	6	85.8	1.2	2.0	89	2	2	97
MG2 - 8	5.6.E+04	b.d.	b.d	803	0.22	74.18	1.05	0.0487	0.0012	0.0903	0.0025	0.0135	0.0002	0.51	112	53	59	7	86.3	1.2	2.0	88	2	3	98

Table S2 (continued): Laser ablation SC–SF–ICP–MS U–Pb zircon data.

Identifier	206Pb (CPS)	204Pb (CPS)	206Pb/204Pb	U (mg/g)	Th/U	Data for Tera-Wasserburg plot				Data for Wetherill plot					Dates (Ma)									Concordance (%)
						238U/206Pb	2 s	$^{207}Pb/^{206}Pb$	2 s	$^{207}Pb/^{235}U$	2 s	$^{206}Pb/^{238}U$	2 s	rho	$^{207}Pb/^{206}Pb$	2 s	$2s_{sys}$		$^{206}Pb/^{238}U$	2 s	$2s_{sys}$	$^{207}Pb/^{235}U$	2 s	$2s_{sys}$	206/238 - 207/235
MG2 - 9	7.2.E+04	b.d.	b.d	1123	0.14	75.70	1.20	0.0484	0.0013	0.0880	0.0026	0.0132	0.0002	0.54	113	58	64	8	84.6	1.3	2.0	86	3	3	99
MG2 - 12	5.7.E+04	b.d.	b.d	924	0.28	76.05	1.68	0.0521	0.0019	0.0934	0.0035	0.0132	0.0003	0.59	264	78	84	9	84.2	1.9	2.4	91	3	4	93
MG2 - 13	3.9.E+04	b.d.	b.d	582	0.19	73.31	1.24	0.0548	0.0016	0.1021	0.0035	0.0136	0.0002	0.49	383	68	69	10	87.4	1.5	2.1	99	3	4	89
MG2 - 15	7.9.E+04	b.d.	b.d	1291	0.11	75.82	1.44	0.0497	0.0015	0.0888	0.0027	0.0132	0.0003	0.62	162	63	71	11	84.5	1.6	2.2	86	3	3	98
Ples - 1	1.7.E+05	b.d.	b.d	555	0.10	18.53	0.24	0.0538	0.0007	0.4006	0.0070	0.0540	0.0007	0.74	349	30	32		339	4.3	7.4	342	5	8	99
Ples - 2	1.8.E+05	b.d.	b.d	571	0.10	18.67	0.24	0.0531	0.0007	0.3926	0.0071	0.0536	0.0007	0.71	323	30	33		336	4.2	7.3	336	5	8	100
Ples - 3	1.5.E+05	b.d.	b.d	491	0.10	18.78	0.25	0.0534	0.0008	0.3919	0.0071	0.0532	0.0007	0.75	333	33	35		334	4.4	7.3	336	5	7	100
Ples - 6	1.6.E+05	b.d.	b.d	522	0.10	18.72	0.25	0.0537	0.0009	0.3951	0.0078	0.0534	0.0007	0.67	344	36	38		335	4.3	7.4	338	6	8	99
Ples - 7	1.5.E+05	b.d.	b.d	468	0.10	18.81	0.24	0.0537	0.0009	0.3926	0.0078	0.0532	0.0007	0.65	341	38	39		334	4.2	7.3	336	6	8	99
Ples - 8	1.7.E+05	b.d.	b.d	544	0.10	18.83	0.25	0.0530	0.0008	0.3880	0.0075	0.0531	0.0007	0.68	314	35	37		334	4.3	7.3	333	6	8	100
Ples - 9	1.7.E+05	b.d.	b.d	548	0.10	18.55	0.24	0.0527	0.0008	0.3914	0.0071	0.0539	0.0007	0.71	301	33	36		339	4.2	7.3	335	5	8	101
Ples - 10	1.7.E+05	b.d.	b.d	552	0.10	18.67	0.24	0.0529	0.0008	0.3906	0.0073	0.0536	0.0007	0.69	309	34	37		336	4.2	7.3	334	5	8	101
Ples - 11	1.7.E+05	b.d.	b.d	571	0.10	18.51	0.24	0.0534	0.0008	0.3984	0.0074	0.0540	0.0007	0.70	332	32	34		339	4.3	7.4	340	5	8	100
Ples - 12	1.7.E+05	b.d.	b.d	574	0.10	18.71	0.24	0.0536	0.0008	0.3951	0.0073	0.0535	0.0007	0.71	338	32	34		336	4.3	7.3	338	5	8	99
Ples - 13	1.7.E+05	b.d.	b.d	556	0.10	18.60	0.25	0.0533	0.0008	0.3950	0.0072	0.0538	0.0007	0.72	330	33	35		338	4.3	7.3	338	5	8	100
Ples - 14	1.7.E+05	b.d.	b.d	567	0.10	18.60	0.24	0.0530	0.0007	0.3928	0.0067	0.0538	0.0007	0.75	317	30	33		338	4.2	7.3	336	5	8	100
Ples - 15	1.8.E+05	b.d.	b.d	610	0.10	18.64	0.25	0.0534	0.0008	0.3956	0.0070	0.0537	0.0007	0.75	333	33	35		337	4.3	7.3	339	5	7	100
Ples - 16	1.7.E+05	b.d.	b.d	566	0.10	18.49	0.24	0.0539	0.0007	0.4018	0.0071	0.0541	0.0007	0.72	353	30	32		340	4.2	7.3	343	5	8	99
Ples - 17	1.6.E+05	b.d.	b.d	544	0.10	18.67	0.24	0.0530	0.0008	0.3911	0.0073	0.0536	0.0007	0.70	314	35	37		336	4.3	7.3	335	5	8	100
Ples - 18	1.7.E+05	b.d.	b.d	594	0.10	18.77	0.25	0.0543	0.0008	0.4006	0.0073	0.0533	0.0007	0.72	374	32	35		335	4.3	7.3	342	5	8	98
Ples - 19	1.7.E+05	b.d.	b.d	580	0.10	18.67	0.24	0.0535	0.0008	0.3966	0.0073	0.0536	0.0007	0.71	342	33	35		336	4.3	7.3	339	5	8	99
Ples - 20	1.7.E+05	b.d.	b.d	595	0.10	18.78	0.24	0.0544	0.0008	0.4007	0.0074	0.0533	0.0007	0.70	372	34	36		334	4.2	7.3	342	5	8	98
Ples - 21	1.8.E+05	b.d.	b.d	594	0.11	18.81	0.24	0.0526	0.0007	0.3873	0.0070	0.0532	0.0007	0.72	299	31	33		334	4.2	7.2	332	5	8	101
Ples - 22	1.6.E+05	b.d.	b.d	532	0.10	18.72	0.25	0.0539	0.0008	0.3985	0.0073	0.0534	0.0007	0.72	351	34	36		336	4.3	7.3	341	5	8	99
Ples - 23	1.7.E+05	b.d.	b.d	576	0.10	18.81	0.25	0.0533	0.0008	0.3924	0.0071	0.0532	0.0007	0.73	326	33	35		334	4.3	7.3	336	5	8	99
Ples - 24	1.7.E+05	b.d.	b.d	568	0.10	18.67	0.24	0.0532	0.0008	0.3921	0.0071	0.0536	0.0007	0.71	320	33	36		336	4.2	7.3	336	5	7	100
Ples - 25	1.7.E+05	b.d.	b.d	588	0.10	18.87	0.25	0.0528	0.0008	0.3867	0.0070	0.0530	0.0007	0.72	308	32	34		333	4.2	7.2	332	5	8	100
Ples - 26	1.8.E+05	b.d.	b.d	626	0.10	18.59	0.24	0.0535	0.0007	0.3975	0.0071	0.0538	0.0007	0.72	338	32	33		338	4.2	7.3	339	5	8	99
Ples - 27	1.6.E+05	b.d.	b.d	578	0.10	18.67	0.24	0.0536	0.0008	0.3945	0.0074	0.0536	0.0007	0.69	336	33	36		336	4.2	7.2	338	5	7	99
Ples - 28	1.6.E+05	b.d.	b.d	563	0.10	18.64	0.24	0.0532	0.0008	0.3921	0.0076	0.0537	0.0007	0.67	322	36	38		337	4.3	7.4	335	6	8	100
Ples - 29	1.6.E+05	b.d.	b.d	602	0.10	18.74	0.24	0.0541	0.0008	0.3959	0.0075	0.0534	0.0007	0.68	359	33	35		335	4.2	7.2	338	5	8	99
Ples - 30	1.7.E+05	b.d.	b.d	635	0.10	18.90	0.24	0.0534	0.0008	0.3881	0.0072	0.0529	0.0007	0.69	331	33	35		332	4.1	7.2	333	5	8	100
Ples - 31	1.6.E+05	b.d.	b.d	599	0.10	18.35	0.24	0.0535	0.0008	0.3988	0.0075	0.0545	0.0007	0.68	337	34	37		342	4.3	7.4	341	6	7	100
Ples - 32	1.8.E+05	b.d.	b.d	674	0.10	18.52	0.24	0.0535	0.0008	0.3957	0.0070	0.0540	0.0007	0.73	336	32	34		339	4.3	7.3	338	5	8	100

Uncertainties quoted without components related to systematic error unless otherwise stated. Total systematic uncertainties (s sys): $^{206}Pb/^{238}U$ = 1.8 %; $^{207}Pb/^{206}Pb$ = 0.5 (2s).
a Data not corrected for common Pb
b Concordance calculated as: (206Pb-238U date/207Pb-235U date)*100

Table S3: Compositions of the prehnite–pumpellyite mineral from metamorphic sole rocks.

Rock Type	**Prehnite-Pumpellyite amphibole schist**									
Type	**Prehnite**					**Pumpellyite**				
SAMPLE	**M4P-1**	**M4P-2**	**M4P-3**	**M4P-4**	**M4P-5**	**M4PR-1**	**M4PR-2**	**M4PR-3**	**M4PR-4**	**M4PR-5**
SiO_2	37.48	37.34	37.54	37.31	37.58	43.26	43.32	43.17	43.25	43.33
TiO_2	0.12	0.45	0.25	1.06	0.21	0	0	0	0	0.07
Al_2O_3	26.52	25.74	25.99	25.48	26.28	24.71	24.7	24.61	24.57	24.54
FeO	2.29	2.77	2.65	2.37	2.54	0.04	0.04	0.07	0.05	0.05
MnO	0.03	0.02	0.02	0.02	0.03	0	0	0.03	0	0
MgO	3.04	2.9	3.03	3.1	2.82	0	0	0	0	0
CaO	23.32	23.35	23.35	23.71	23.65	27.71	27.71	27.6	27.66	27.58
Na_2O	0	0.03	0.02	0	0	0	0	0.02	0	0
K_2O	0.02	0.02	0.03	0.02	0.02	0	0.01	0	0	0
TOTAL	93.03	92.92	93.19	93.31	93.48	95.72	95.82	95.5	95.53	95.57
Si	5.37	5.38	5.39	5.35	5.38	5.95	5.95	5.95	5.96	5.97
Al^{total}	4.48	4.37	4.40	4.31	4.44	4.01	4.00	4.00	3.99	3.98
Ti	0.01	0.05	0.03	0.11	0.02	0	0	0	0	0.01
Fe	0.27	0.33	0.32	0.28	0.3	0	0	0.01	0.01	0.01
Mg	0.65	0.62	0.65	0.66	0.6	0	0	0	0	0
Ca	3.58	3.61	3.59	3.65	3.63	4.08	4.08	4.08	4.08	4.07
TOTAL	18.38	18.39	18.39	18.38	18.38	18.05	18.04	18.05	18.04	18.03

Number of ions on the basis of 6 oxygens. Total Fe is expressed as FeO*.